Numerical Studies of sub-Keplerian Accretion Disk onto Black Holes

Sudip K. Garain

KASI, 3rd May, 2019

Plan of talk

- Introduction
- Basics of accretion process
- Observational results
- Theoretical models and our simulations

Some historical background

PHYSICAL REVIEW
LETTERS

VOLUME 9 DECEMBER 1, 1962 NUMBER 11

EVIDENCE FOR X RAYS FROM SOURCES OUTSIDE THE SOLAR SYSTEM*

Riccardo Giacconi, Herbert Gursky, and Frank R. Paolini
American Science and Engineering, Inc., Cambridge, Massachusetts

and

Bruno B. Rossi
Massachusetts Institute of Technology, Cambridge, Massachusetts
(Received October 12, 1962)

Data from an Aerobee rocket carrying a payload consisting of three large area Geiger counters have revealed a considerable flux of radiater was placed in a well formed by an anticoincidence scintillation counter designed to reduce the cosmic-ray background. The experiment was in-

VOLUME 11, NUMBER 12 PHYSICAL REVIEW LETTERS 15 DECEMBER 1963

FURTHER EVIDENCE FOR THE EXISTENCE OF GALACTIC X RAYS*

Herbert Gursky, Riccardo Giacconi, and Frank R. Paolini
American Science and Engineering, Inc., Cambridge, Massachusetts

and

Bruno B. Rossi
Massachusetts Institute of Technology, Cambridge, Massachusetts
(Received 26 September 1963)

In a previous Letter[1] we reported experimental evidence for the existence of x-ray sources outside the solar system. We have since performed two rocket experiments, using similar instrumentation, from the White Sands Missile Range, New Mexico, in October 1962 and June 1963. These flights have furnished

was provided with collimators limiting the angle of incidence of a maximum of 20°. The (area) ×(solid angle) factor for this detector was 1.6 cm^2 sr for low-energy particles and increased to 110 cm^2 sr for cosmic rays. Aspect was determined from a combination of optical sensors and flux gate magnetometers.

- Also, around this time, Roy Kerr published his solution
- John Wheeler coined the name black holes in 1967; before that these objects were called collapsed stars or collapsers
- Lynden-Bell in 1969 made strong argument that accretion close to Eddington rate onto super-massive black holes must be responsible for such high luminosity from quasars
- First astrophysics related satellite UHURU was launched in 1970; Cygnus X-1 was observed carefully
- Detail analysis of spectra of stars and quasi-stellar objects (QSOs) demanded that angular momentum of accreting matter must be taken into account; Shakura-Sunyaev stardard disk model in 1973

Black Hole Binaries

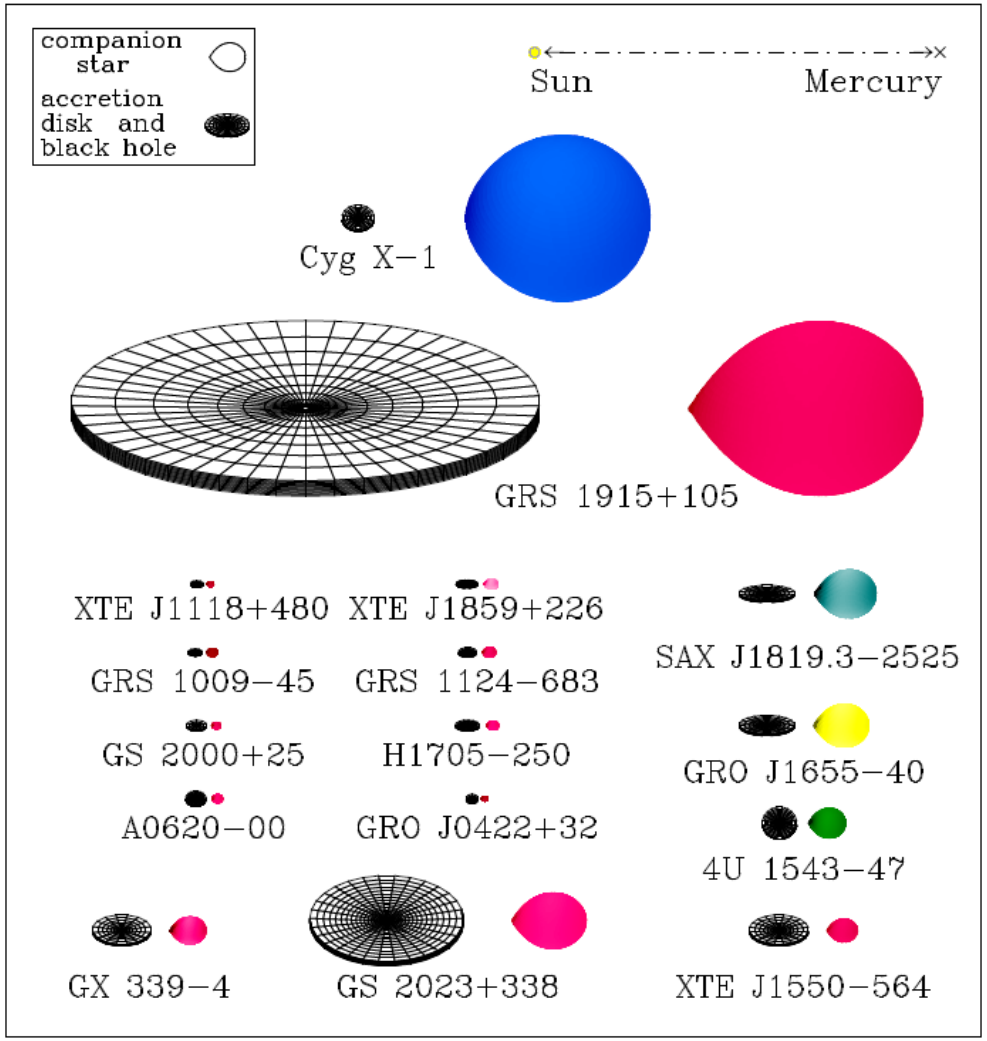

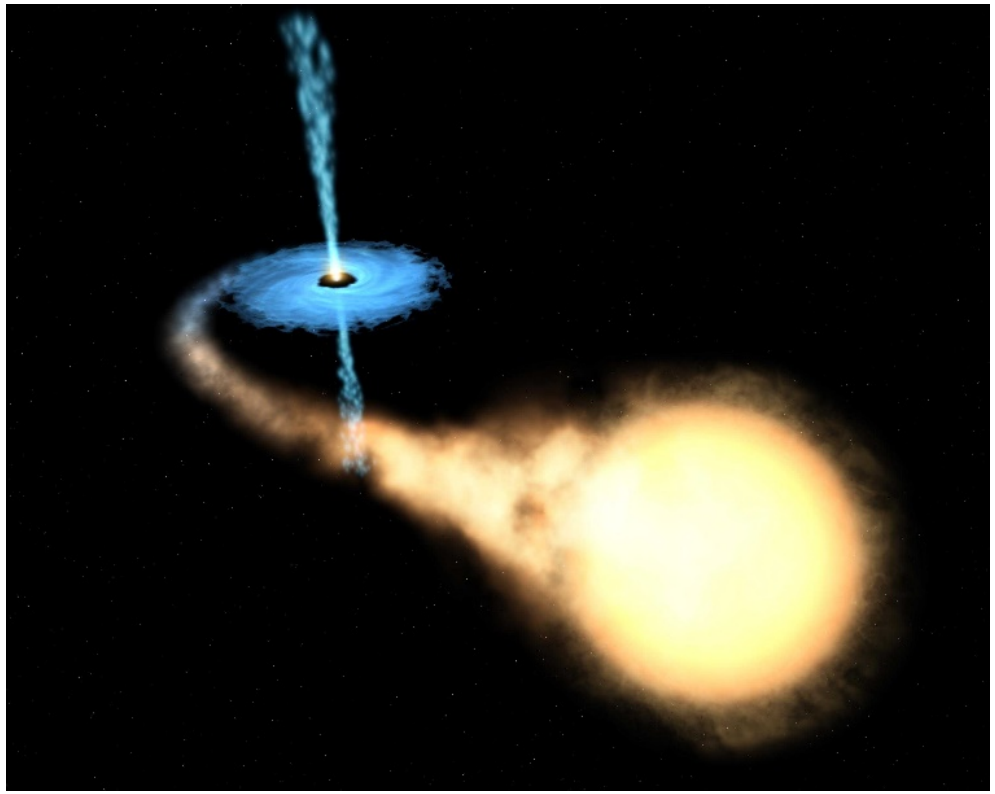

Black hole binaries in our Milky Way (Remillard & McClintock, 2006)

In case of binary systems, mass transfer from the companion to the compact object can take place in two ways:

1) **Roche Lobe overflow**
2) **Wind accretion from companion**

For black holes at the galactic centers, a third possibility is tidal disruption of a nearby star.

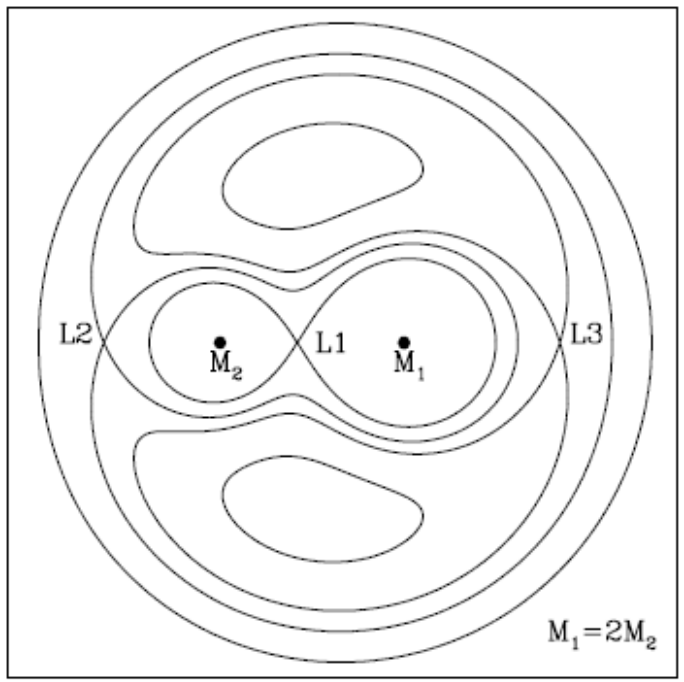

$$\Phi_{eff}(r) = -\frac{M_1}{|r - r_1|} - \frac{M_2}{|r - r_2|} - \frac{1}{2}|\Omega \times r|$$

Figure 1.1: Equipotential surfaces of a compact binary system with mass ratio $M_1/M_2 = 2$. Distances are in units of GM_1/c^2. L_1, L_2 and L_3 are called the Lagrange points where Φ_{eff} is locally or globally an extremum. Roche lobe overflow occurs when matter from M_2 fills its lobe (left section of the figure-of-eight formed by the innermost contour) and passes through L_1 to the star M_1 on the right.

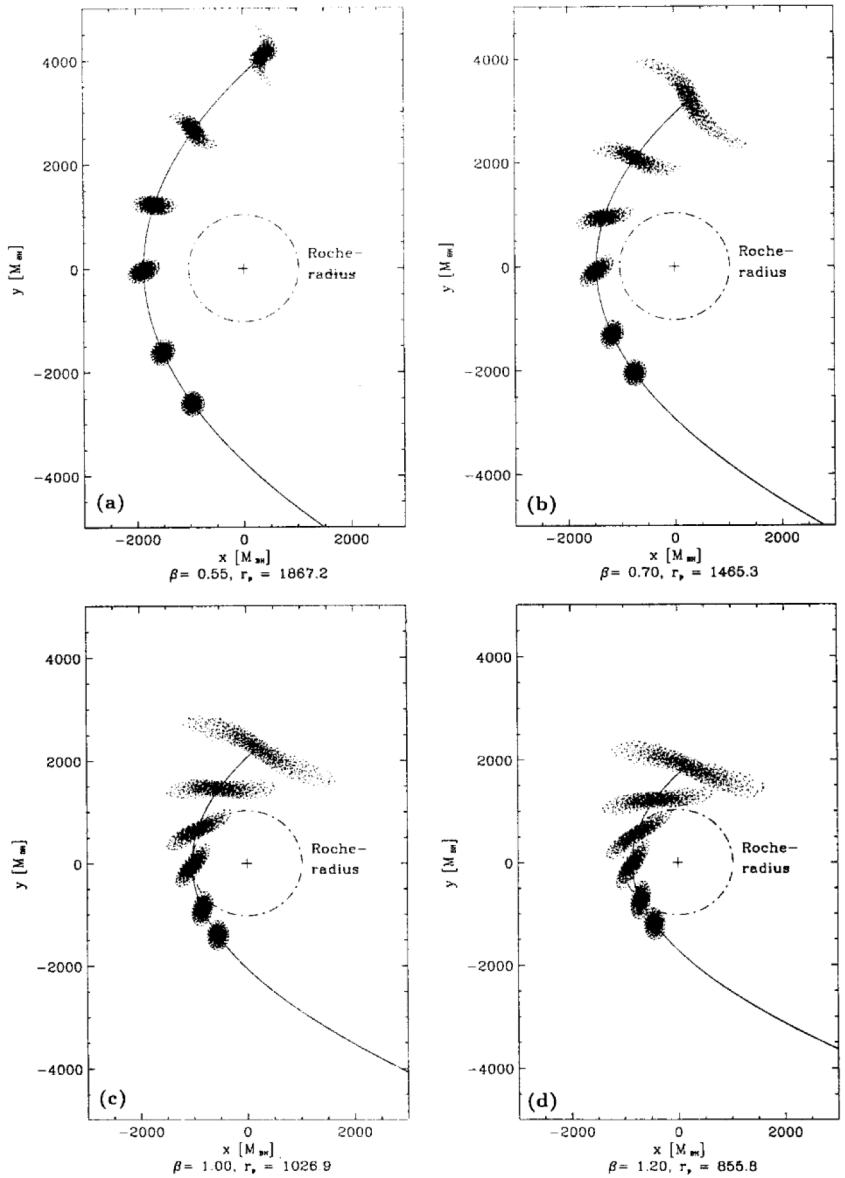

- **Accretion onto black holes are necessarily transonic. Matter crosses the horizon with speed of light, whereas the maximum sound speed is 1/3 of the speed of light (S. Weinberg, Gravitation and Cosmology, chapter 2.10).**

- **Gravitational energy release is the primary source of radiation for compact objects (neutron star, black hole, white dwarf).**

If a particle of mass "m" move from radius r_1 to r_2 towards a star of mass "M", gravitational energy release is

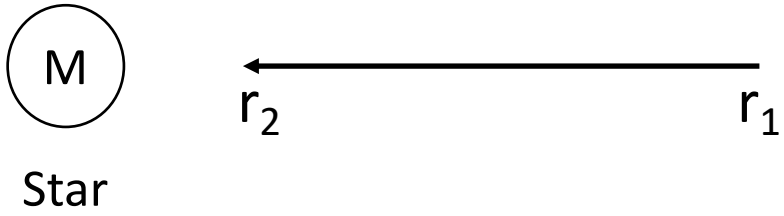

$$dE = -GMm/r_1 - (-GMm/r_2)$$

If $r_1 = \infty$ and $r_2 = r^*$, where r^* is the radius of the star, then $dE = GMm/r^*$.

For a neutron star of radius 10KM and mass of one solar mass, $dE \sim 10^{20}$ erg/gm

- **For a proton-electron pair, if this gravitational energy is ENTIRELY converted to thermal energy, then we can estimate the temperature of the pair in optically thin limit. It turns out:**

$kT \sim 50$ MeV or $T \sim 5.\ 10^{11}$ K

In reality the efficiency is much less!!!

Radiation mechanisms

Radiation from an accretion disk covers entire electro-magnetic spectrum ranging from radio to high energy gamma rays. Some relevant emission mechanism are as follows:

1. **Blackbody radiation: Mostly by the optically thick standard thin disk**

2. **Bremsstrahlung radiation (free-free emission):**

When a charged particle moves in the Coulomb field of another charged particle, the electric field causes the moving particle to emit bremsstrahlung. The radiation from a highly ionized medium which is in local thermal equilibrium (particles have Maxwell-Boltzmann velocity distribution) and optically thin (so that the radiation field is not in equilibrium), has a characteristic shape of continuous spectrum that is determined only by the temperature. This particular type of bremsstrahlung process is called the thermal bremsstrahlung.

$$I(\nu, T) = 6.8 \times 10^{-38} Z^2 n_e n_i T^{-1/2} e^{-n\nu/kT} g(\nu, T) \text{ erg s}^{-1} \text{ cm}^{-3} \text{ Hz}^{-1},$$

3. Thermal Comptonization (inverse-Compton scattering): Photons are mainly energized by this process inside the accretion disks.

For non-relativistic electrons in thermal equilibrium at temperature T, the expression for the energy transfer per scattering is given by (RL79),

$$\frac{(\Delta h\nu)_{NR}}{h\nu} = \frac{(4kT - h\nu)}{m_e c^2}.$$

emitted spectrum depends upon the factor $y = \tau_{es}(\Delta h\nu)_{NR}/h\nu$, where, τ_{es} is the electron scattering optical depth.

4. Synchrotron radiation: Non-thermal radiation. When the velocity of the electrons gyrating in the magnetic field is relativistic (v ~ c), the radiation emitted is called synchrotron radiation. The energy spectrum of synchrotron radiation results from the superposition of the individual electron spectra, and the energy spectrum can be approximated as power law distribution, i.e., $N(E) \propto E^{-p}$.

The synchrotron radiation is self-absorbed by electrons up to some critical frequency (the *turnover frequency*) ν_t, above which plasma becomes optically thin to the synchrotron radiation, i.e.

$$\tau = \alpha_{\nu_t} R = 1 \qquad (12)$$

where R is the characteristic size of the plasma. Below ν_t, the observed emission has the blackbody, typically Rayleigh-Jeans, spectrum. Equation (12) with α_{ν_t} calculated from Kirchoff's law can be solved for ν_t numerically. For an approximate, analytical expression see Zdziarski et al. (1998).

5. Non-Thermal Compotonization: Electrons may be energized at the shock front by the shock acceleration process (Blandford & Eichler 1987; Chakrabarti 1996) very close to the black hole, where their kinetic energy become very high. The effect of non-thermal electrons on Comptonization will produce a high energy tail in the spectrum that is above the thermal cut-off.

In addition to these, there are may be other emission mechanisms e.g., line emission (Fe-K line is observed in X-ray spectrum).

Eddington luminosity:

- **Radiation from the accreting matter exert outward radiation pressure on electrons.**
- **Gravity pulls the protons.**
- **The balance between these two forces determine the definition of Eddington luminosity**

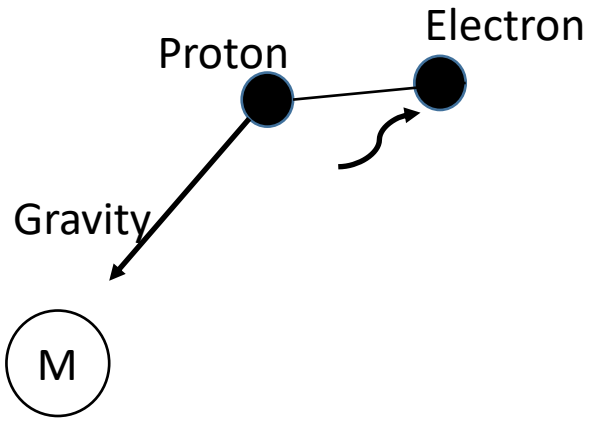

$m_e/m_p \cong 5 \times 10^{-4}$ is the ratio of the electron and proton masses. If S is the radiant energy flux (erg $s^{-1}cm^{-2}$) and $\sigma_T = 6.7 \times 10^{-25}$ cm^2 is the Thomson cross-section, then the outward radial force on each electron equals the rate at which it absorbs momentum, $\sigma_T S/c$. If there is a substantial population of elements other

the radiation pushes out electron–proton pairs against the total gravitational force $GM(m_p + m_e)/r^2 \cong GMm_p/r^2$ acting on each pair at a radial distance r from the centre. If the luminosity of the accreting source is L(erg s^{-1}), we have $S = L/4\pi r^2$ by spherical symmetry, so the net inward force on an electron–proton pair is

$$\left(GMm_p - \frac{L\sigma_T}{4\pi c}\right)\frac{1}{r^2}.$$

There is a limiting luminosity for which this expression vanishes, the Eddington limit,

$$L_{Edd} = 4\pi GMm_p c/\sigma_T \quad (1.3)$$

$$\cong 1.3 \times 10^{38}(M/M_\odot)\,\text{erg s}^{-1}. \quad (1.4)$$

Mass Eddington rate:
$m_{Edd} = L_{Edd} / c^2$

Units:

Length scale: $2GM/c^2$ or GM/c^2 . For a 10 solar mass black hole, $2GM/c^2$ = 30 KM

Time scale: Length scale / speed of light (~10^{-4} sec)

Velocity: speed of light

Angular momentum: Length scale * speed of light

Typical X-ray Observations from Black Hole Binaries

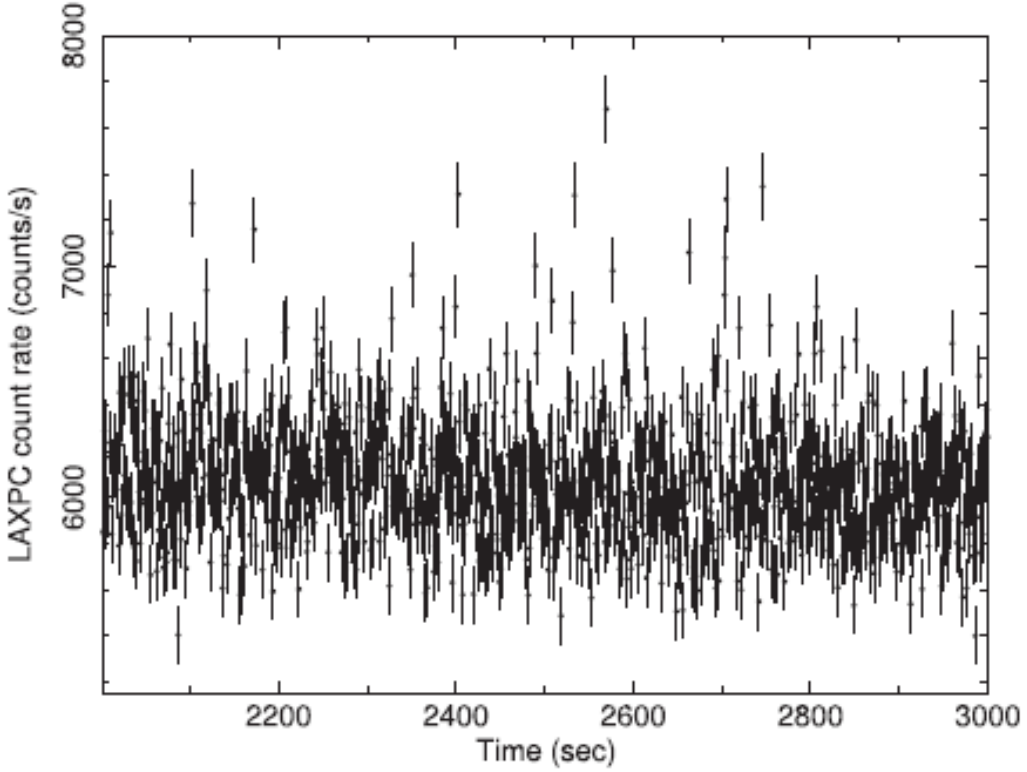

Figure 1. Typical 1 ksec light curve of the χ class in the energy range of 3.0–80.0 keV is shown where count rate from all three LAXPC detectors—LAXPC10, LAXPC20, and LAXPC30 are combined.

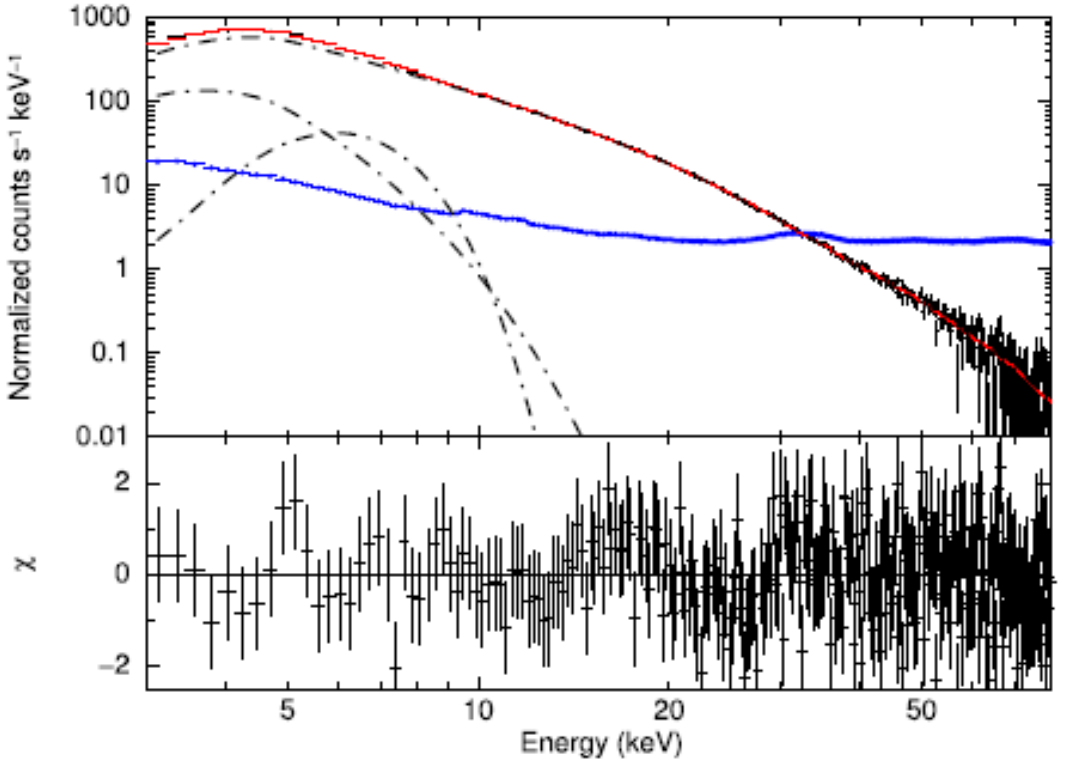

Figure 2. Top panel shows counts spectrum as observed from LAXPC10 for the orbit number 2363, fitted with a model consisting of a disk blackbody, thermal Comptonization and a broad iron line. Resultant model spectra is shown by the red line, while the thick blue line represents the expected background level.

Typical X-ray Observations from Black Hole Binaries

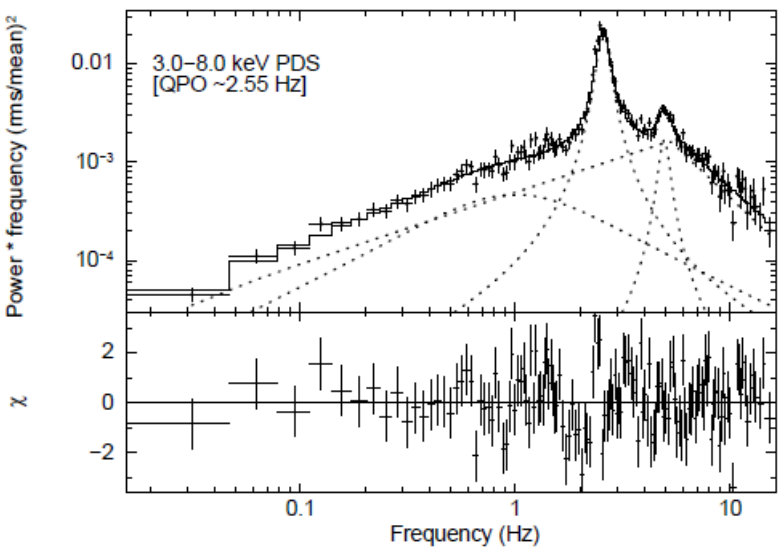

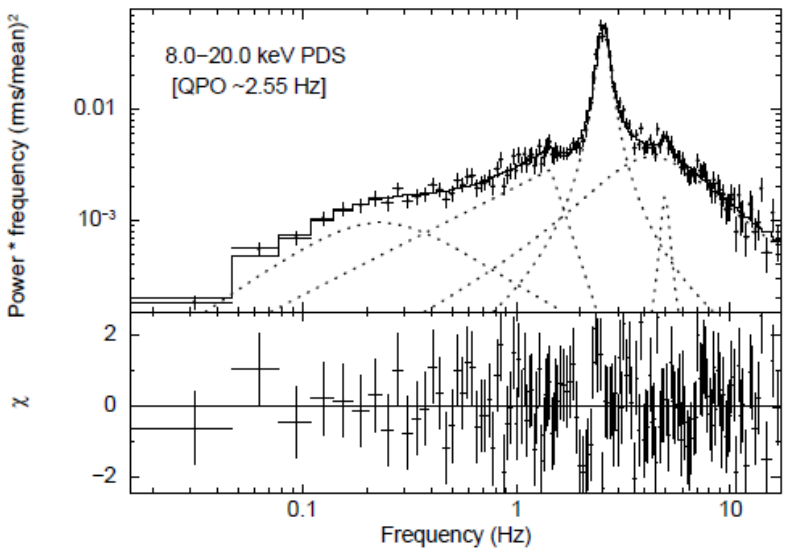

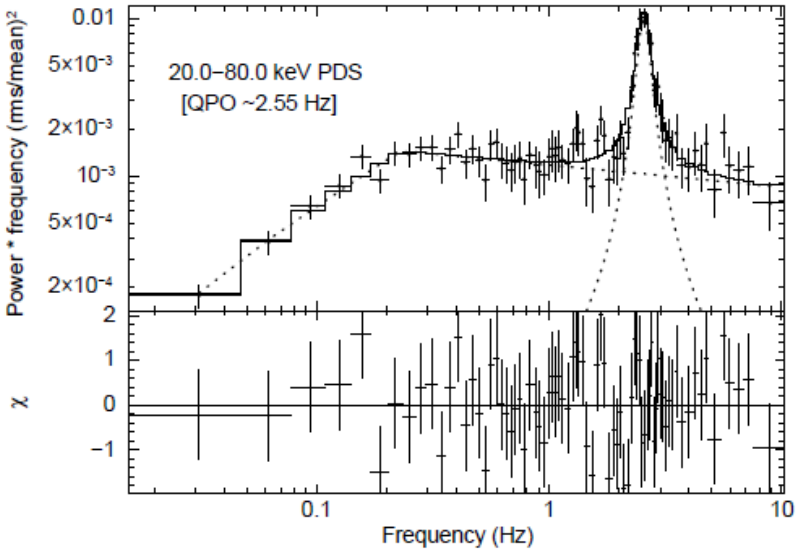

Power-density spectra of the above lightcurve in three different energy ranges (Yadav et al, ApJ, 2016).

Spectral states: hard, soft

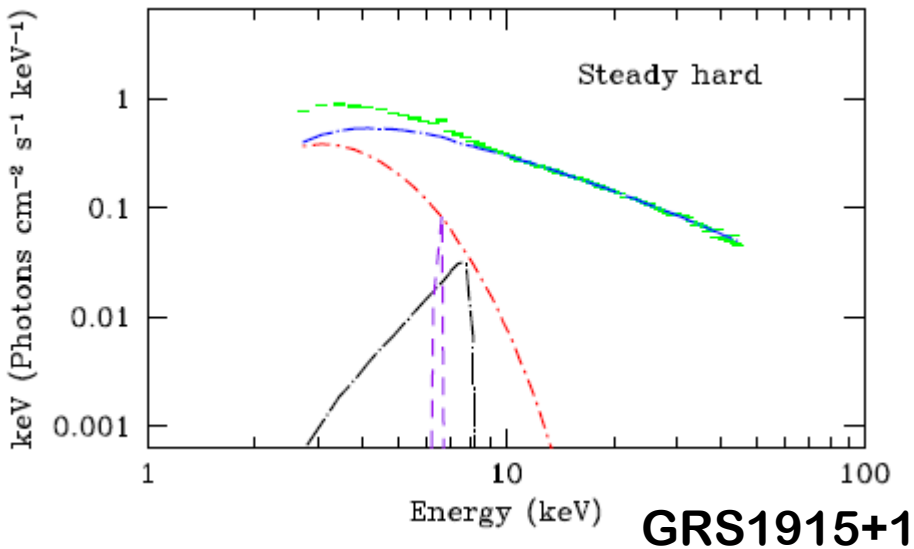

GRS1915+105

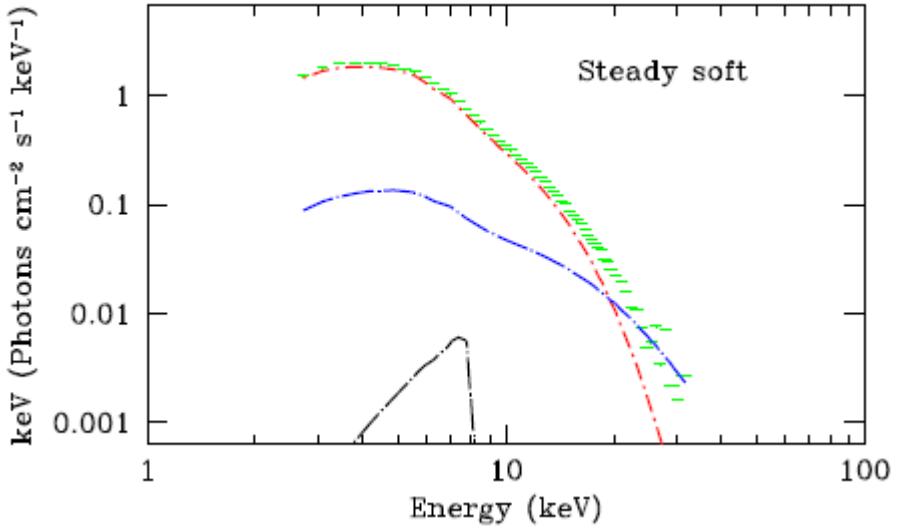

Two unfolded spectra which are typical and exemplify the steady-hard and steady-soft data, respectively. Top: the steady-hard spectrum for data segment 1103_a (ObsID 20402-01-10-00). Bottom: the steady-soft spectrum for data segment 0881_a (ObsID 10408-01-11-00). Data is represented in green, the disk component in red, and the coronal component in blue. Notethe curvature in both coronal components. (**Peris et al., ApJ, 2018**)

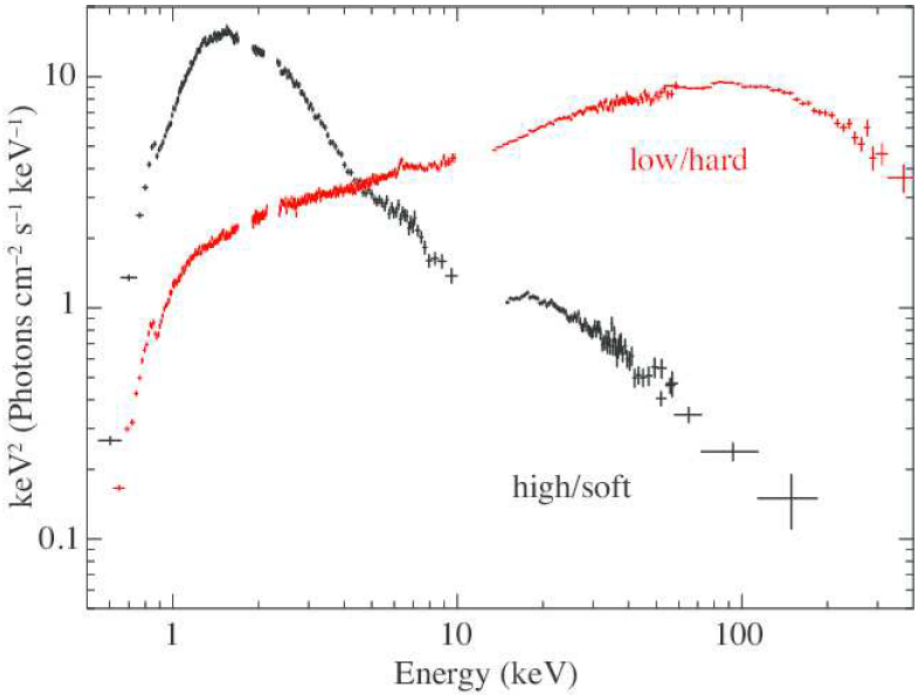

Suzaku spectra of black hole candidate Cygnus X-1. The black one was obtained in the high/soft state on 2010 December 16 and the red one was taken in the low/hard state on 2005 October 5 (**Yamada et al., PASJ, 2013)**

Image of event horizon using EHT

Theoretical models: Magnetized accretion flow onto black holes (initial poloidal magnetic field).

- **Magnetically Arrested Disk (MAD): When the field strength is high, the inner accretion disk is disrupted; blobs of matter is accreted with velocity much smaller than free-fall velocity; radiatively efficient**

- **Standard and Normal Evolution (SANE): Magnetic field does not build up strong enough; "magnetic field is merely an agent that causes angular momentum transport ('viscosity') but plays no important dynamical role"; standard ADAF system**

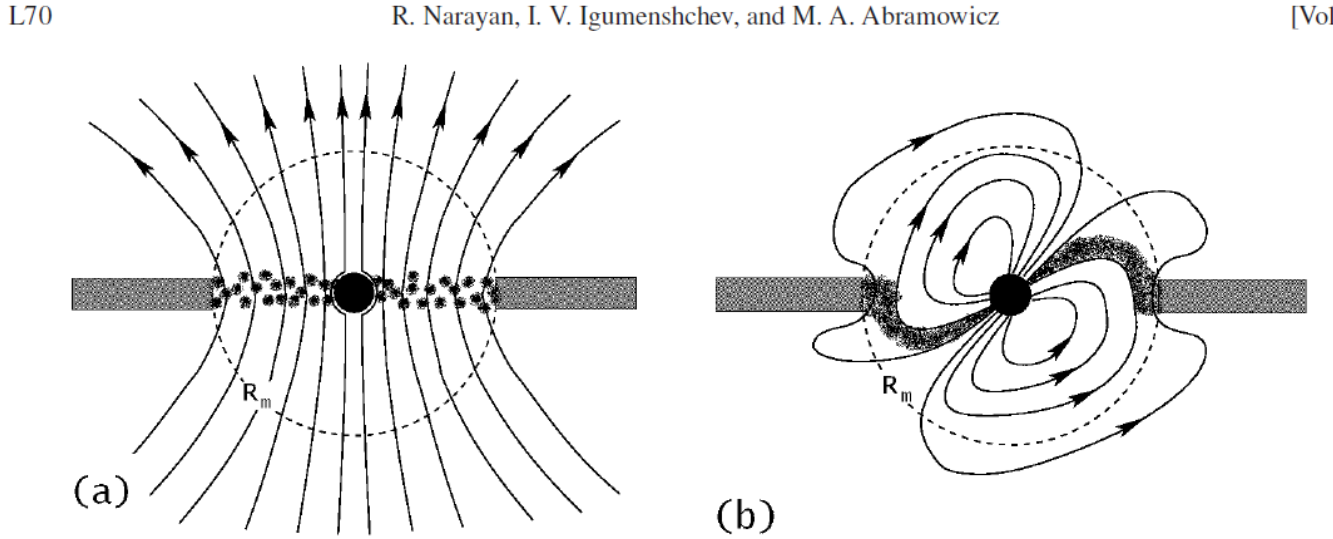

Fig. 1. (a) The basic elements of the proposed accretion model. An axisymmetric accretion disk is disrupted at a magnetospheric radius R_m by a strong poloidal magnetic field which has accumulated at the center. Inside R_m the gas accretes as magnetically confined blobs which diffuse through the field with a relatively low velocity. Surrounding the blobs is a hot low-density corona. (b) The accretion flow around a magnetized compact star. An axisymmetric disk is disrupted at the magnetospheric radius R_m by the strong stellar field. Inside R_m the gas follows the magnetic field lines and free-falls on the polar caps of the star.

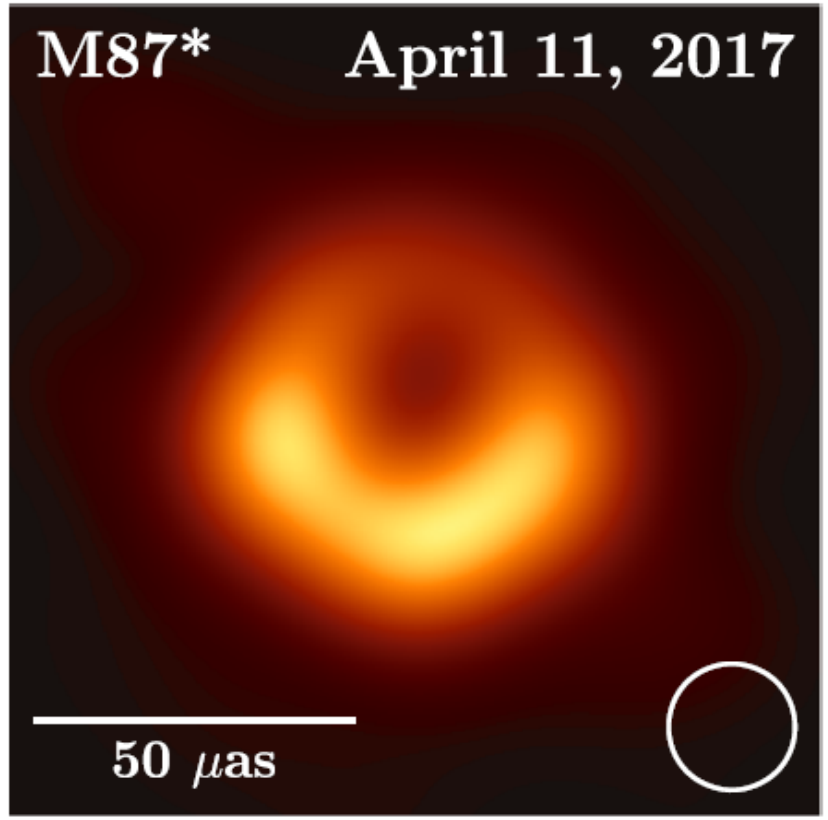

EHT Collaboration, 2019, ApJL

Theoretical Background

Theoretical calculations of accretion onto stars started in 1950s by H Bondi

Theoretical Backgrounds: Spherical Accretion Using Newtonian Potential (1/r)

Let us consider a spherical star of radius R_* surrounded by a spherically symmetric infinite cloud of gas which is rest at infinity. The equation of motion of this infalling matter is given by [80],

$$\frac{\partial u}{\partial t} + u\frac{\partial u}{\partial r} + \frac{1}{\rho}\frac{\partial P}{\partial r} + \frac{1}{r^2} = 0, \tag{2.7}$$

where u is the radial velocity, ρ is the density of the gas, P is the isotropic pressure, r and t are the radial and the time coordinate respectively. The equation is in dimensionless

$a = \sqrt{\gamma P/\rho}$, where γ is the adiabatic index and is equal to $\frac{4}{3}$ in our case.

of state eq. (2.7) could be integrated to obtain the conserved specific energy of the flow:

$$\mathcal{E} = \frac{1}{2}u^2 + na^2 - \frac{1}{r} = na_\infty^2. \tag{2.9}$$

Here, n is the polytropic index, $n = \dfrac{1}{\gamma - 1}$. Integrating eq. (2.8) the mass flux is

Chakrabarti, Physics Report, 1996

The continuity equation where the divergence of the mass flux is equated with the temporal variation of density at a given r, is given by,

$$\frac{\partial \rho}{\partial t} + \frac{1}{r^2}\frac{\partial}{\partial r}(\rho u r^2) = 0. \tag{2.8}$$

Integrating eq. (2.8) the mass flux is obtained as

$$\dot{M} = \rho u r^2. \tag{2.10}$$

a_∞ is its value at infinity, i.e., $a_\infty = \sqrt{\frac{\gamma P_\infty}{\rho_\infty}}$. Using $\rho = (\frac{a^2}{\gamma K})^n$ the eq. (2.10) can be re-written as,

$$\dot{\mathcal{M}} = a^{2n} u r^2. \tag{2.11}$$

Hereafter, the quantity $\dot{\mathcal{M}} = \dot{M}\gamma^n K^n$, which is also conserved in the flow, will be called the 'accretion rate'. Equations (2.9) and (2.11) are the governing equations for two unknowns: $u(r)$ and $a(r)$. Differentiating these equations with respect to r and eliminating $\frac{da}{dr}$ the equation for the velocity variation is obtained as,

$$\frac{du}{dr} = \frac{\frac{1}{r^2} - \frac{2a^2}{r}}{\frac{a^2}{u} - u} = \frac{N}{D}.$$

Mach number M (u/a)

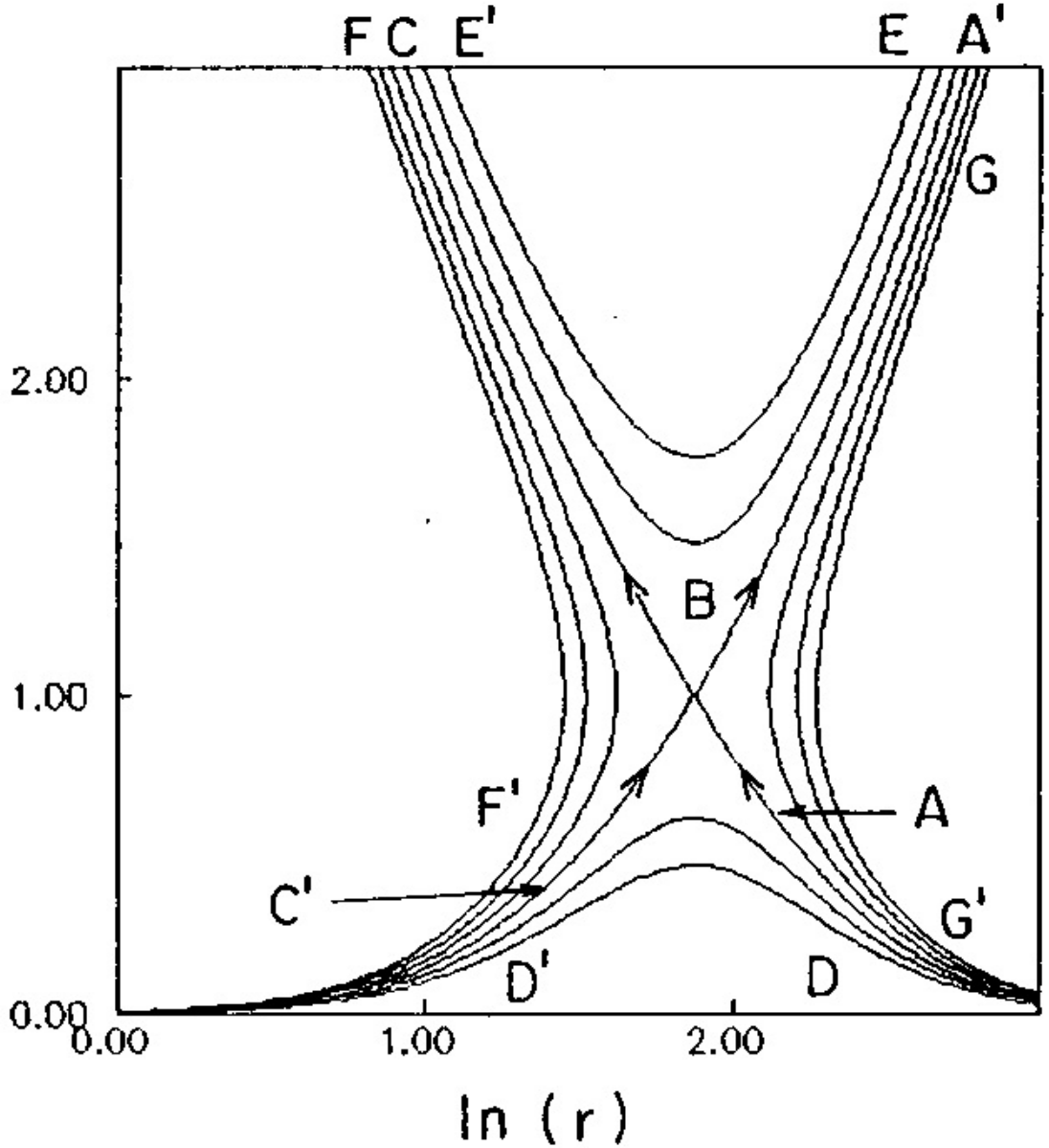

Fig. 2.1a

Shakura-Sunyaev Thin Disk Model

- **One of the famous and very well accepted accretion disk model in this community.**
- **Optically thick and geometrically thin Keplerian disk**

For the steady state disk, the radiation energy flux radiated from the disk surface at radius r is given by (Shapiro & Teukolsky 1983, hereafter ST83),

$$F(r) = 5 \times 10^{26} M_{bh}^{-2} \dot{m}_{17} (2r)^{-3} (1 - \sqrt{\frac{3}{r}}) \text{ erg cm}^{-2} \text{ s}^{-1},$$

where, M_{bh} is the mass of the black hole, $\dot{m}_{17}$ is the mass accretion rate in the units of 10^{17} g s^{-1} and r is in $2GM_{bh}/c^2$ unit.

the local effective temperature is given by (ST83),

$$T_s(r) = [\frac{F(r)}{\sigma}]^{1/4} = 5 \times 10^7 M_{bh}^{-1/2} \dot{m}_{17}^{1/4} (2r)^{-3/4} (1 - \sqrt{\frac{3}{r}})^{1/4} \text{ K}, \qquad (1\text{-}1)$$

- **For stellar mass black holes, the radiation spectrum peaks ~ 1keV, whereas, for supermassive black holes, the radiation spectrum peaks in the UV region.**

Thick, Advective Disk Accretion Using pseudo-Newtonian Potential

- **In presence of angular momentum, the above equations of Bondi accretion change slightly. However the calculation procedures remain same.**

- **Analytical studies show that the sub-Keplerian accretion flow can have more than one sonic points (Fukue 1987, Chakrabarti 1989)**

$$\mathcal{E} = \frac{\vartheta_e^2}{2} + \frac{a_e^2}{\gamma - 1} + \frac{\lambda^2}{2x^2} + g(x),$$

models. Apart from a geometric constant, the conservation equation is given by,

$$\dot{M} = \vartheta_e \rho a^\zeta x^\beta (x-1)^\delta, \qquad (2)$$

where β, ζ and δ are constants. For Model V (see C89), $\beta = 3/2$, $\zeta = 1$, $\delta = 1$. For Model C (see C90), $\beta = 2$, $\zeta = 0$, $\delta = 0$. For Model H (Chakrabarti 1992; Chakrabarti & Molteni 1993), $\beta = 1$, $\zeta = 0$, $\delta = 0$. Note that since the local disc height $h(x)$ depends on sound speed, $h(x) \sim a_e x^{1/2}(x-1)$, and so a factor of a_e^ζ is applicable for this model.

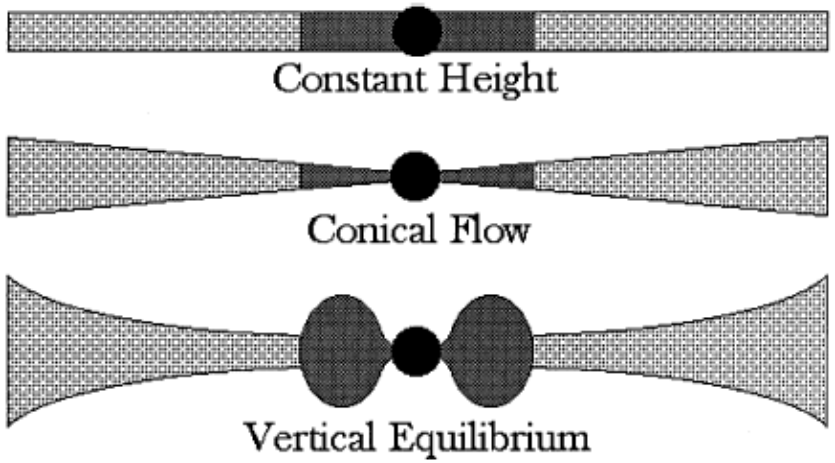

Figure 1. Cartoon diagram of three different models discussed in the text. In a constant-height flow (H), the disc thickness is constant (top). In a conical flow (C), the cross-section in the meridional plane is conical (middle). In a vertical equilibrium flow (V), matter is locally in vertical equilibrium at every point of the disc (bottom).

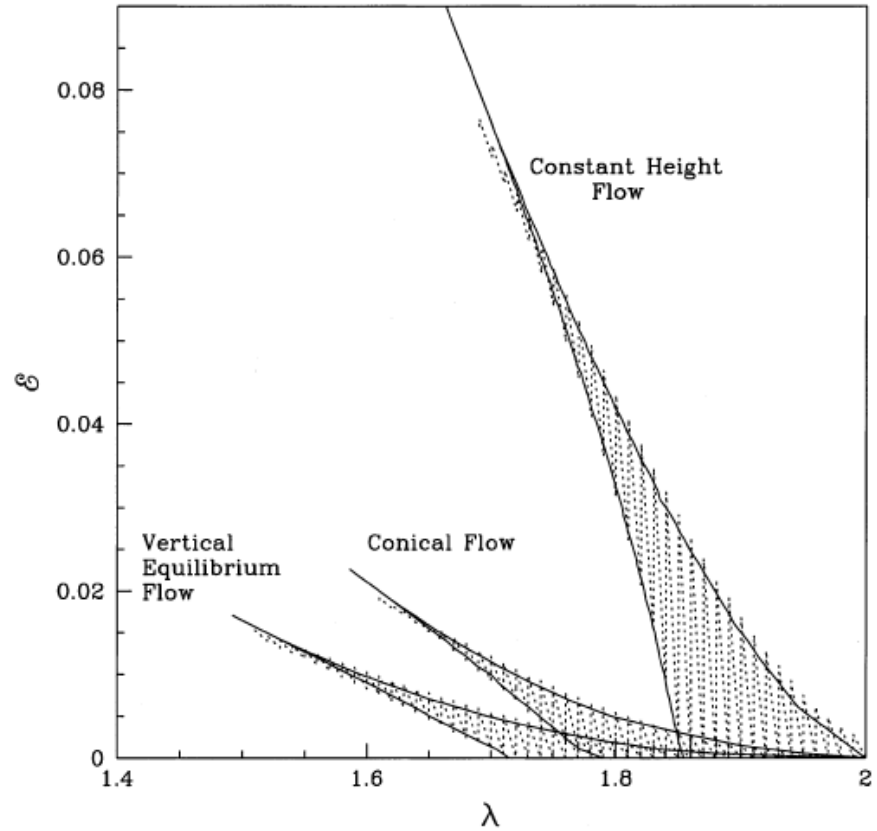

Figure 2. Comparison of the parameter space in three different models in which shocks form. $n_V = n_H = n_C = 3$ is chosen throughout. Solid boundaries are obtained using the numerical method, and shaded regions are obtained using the analytical method.

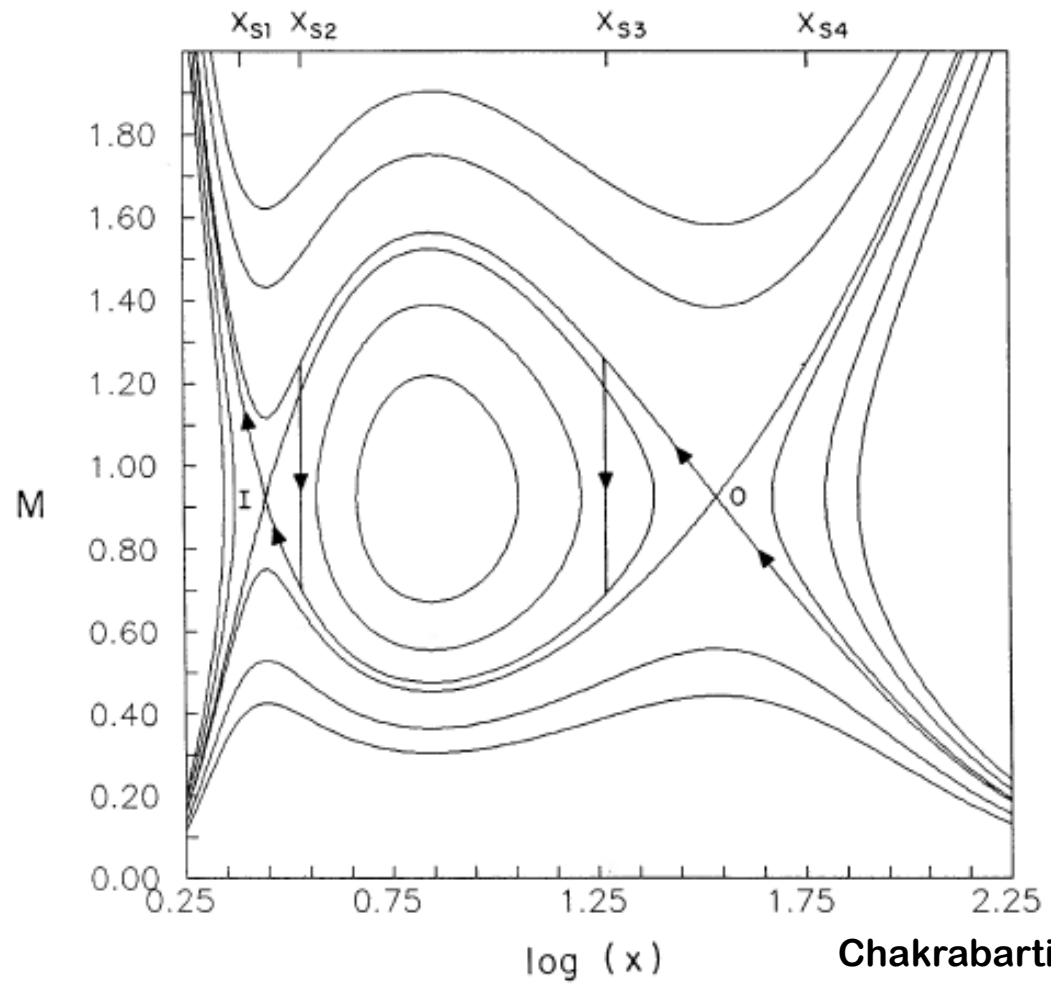

Chakrabarti, 1989

- Analytical solution predicts possibility of shock in accretion flow.
- For a shocked accretion onto black holes, the incoming subsonic flow first passes through the outer sonic point, then passes through a shock and finally must pass through an inner sonic point before getting accreted supersonically
- Many analytical as well as numerical stability analysis of the shock has been performed in latter years

- **We have conducted several numerical tests for 1D, non-dissipative accretion and wind solutions around Schwarzschild and Kerr black holes to verify the possibility of shock formation.**

- **Analytical solution procedures are very much similar for Newtonian and GR cases**

We assume a thin conical wedge shaped adiabatic flow symmetrically placed on both sides of the equatorial plane, $\theta = \pi/2$, entering into a Kerr black hole. For analytical studies, we assume the Kerr metric transformed to the cylindrical coordinate which is written as follows (Novikov & Thorne 1973):

$$\begin{aligned} ds^2 &= g_{\mu\nu} dx^\mu dx^\nu \\ &= -\frac{r^2\Delta}{A} dt^2 + \frac{A}{r^2}(d\phi - \omega dt)^2 + \frac{r^2}{\Delta} dr^2 + dz^2. \end{aligned} \tag{1}$$

Here,

$$A = r^4 + r^2a^2 + 2ra^2,\ \Delta = r^2 - 2r + a^2,\ \omega = 2ar/A,$$

a being the spin parameter of the black hole and ω represents the frame dragging due to the rotation of the central black hole.

In absence of viscosity and any heating or cooling, one can find the conserved specific energy as (Chakrabarti 1996c)

$$\epsilon = hu_t = \frac{1}{1 - na_s^2} u_t, \tag{2}$$

where, $n = 1/(\Gamma - 1)$ is the polytropic index, Γ being the adiabatic index, and $h = 1/\left(1 - na_s^2\right)$ is the enthalpy, a_s being the sound speed. Also,

$$u_t = \left[\frac{\Delta}{(1 - V^2)(1 - \Omega l)(g_{\phi\phi} + l g_{t\phi})}\right]^{1/2}. \tag{3}$$

We rewrite equation (2) as

$$\epsilon = \frac{1}{1 - na_s^2} \frac{1}{\left(1 - V^2\right)^{1/2}} F(r), \tag{7}$$

where,

$$F(r) = \left[\frac{\Delta}{(1 - \Omega l)(g_{\phi\phi} + l g_{t\phi})}\right]^{1/2}.$$

The entropy accretion rate (Chakrabarti 1989, 1996c) can be obtained as

$$\dot{\mu} = \left(\frac{a_s^2}{1 - na_s^2}\right)^n \frac{V}{\left(1 - V^2\right)^{1/2}} G(r), \tag{8}$$

where, $G(r) = r\Delta^{1/2}$.

We follow the standard solution procedures (Chakrabarti 1996a,c) to calculate $V(r)$ and radial dependence of other required quantities. By differentiating equations (7) and (8) with respect to r and eliminating terms involving da_s/dr, we find following expression as the gradient of $V(r)$:

$$\frac{dV}{dr} = \frac{V\left(1 - V^2\right)\left[a_s^2 R_1 - R_2\right]}{\left(V^2 - a_s^2\right)}, \tag{9}$$

where, $R_1 = \frac{1}{G(r)}\frac{dG(r)}{dr}$ and $R_2 = \frac{1}{F(r)}\frac{dF(r)}{dr}$.

At the sonic point, both numerator and the denominator vanish and one obtains the so-called sonic point condition as

$$V_c = a_{s,c}; \quad a_{s,c}^2 = \left.\frac{R_2}{R_1}\right|_c. \tag{10}$$

Here, subscript c refers to the quantities evaluated at the sonic point $r = r_c$.

To find a complete solution from the horizon to infinity for a given black hole spin parameter a, one needs to supply the specific energy ε and the specific angular momentum l. For Kerr black holes, a

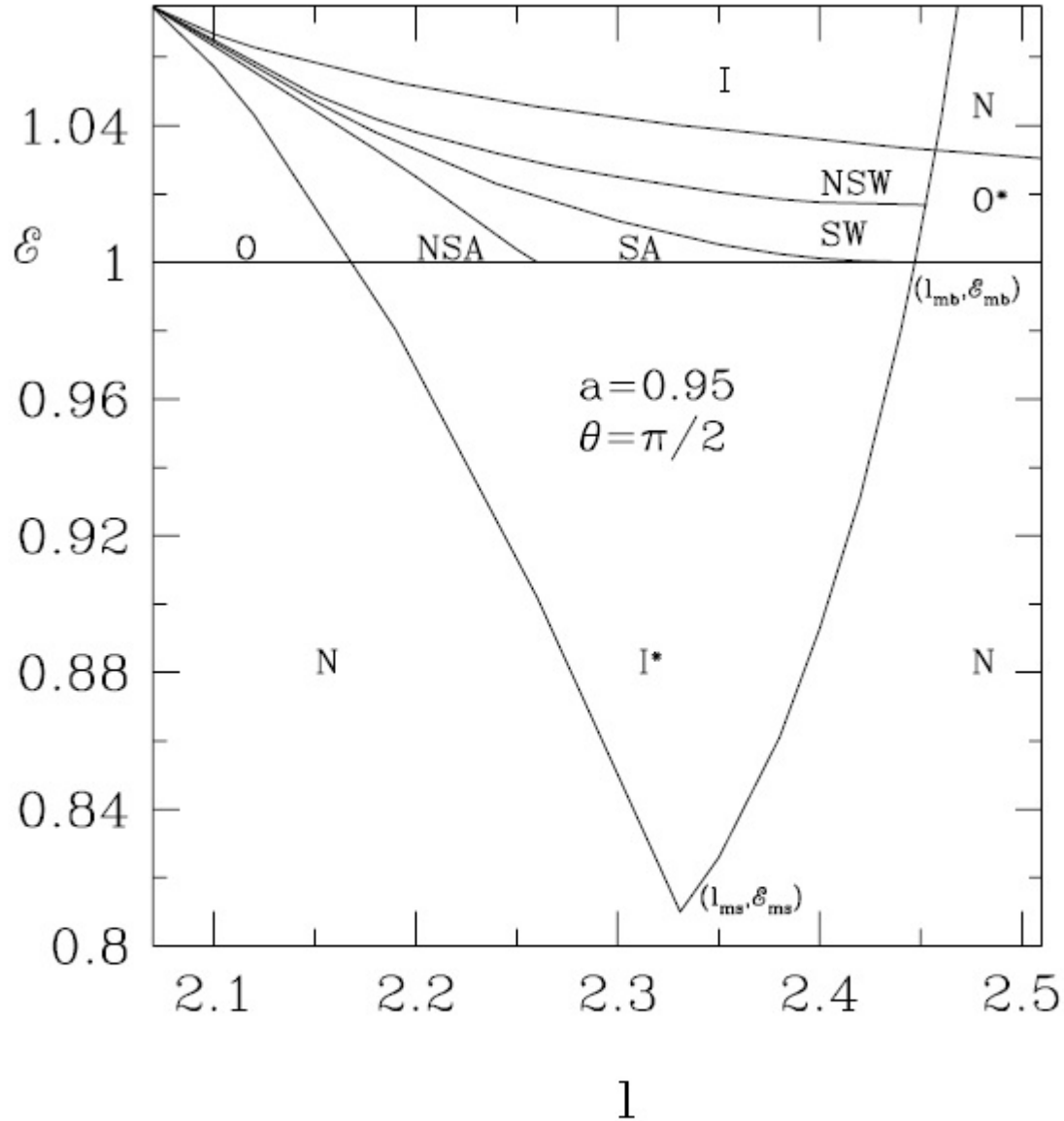

FIG. 2.—Classification of the entire parameter space spanned by the specific energy and angular momentum in terms of the number of sonic points and the presence or absence of shocks. See § 4.1 for details.

NSA : No Shock in Accretion
SA : Shock in Accretion
SW : Shock in Wind
NSW : No Shock in Wind

Chakrabarti, ApJ, 1996

Results: One Dimensional Bondi Flow

Schwarzschild Space-time

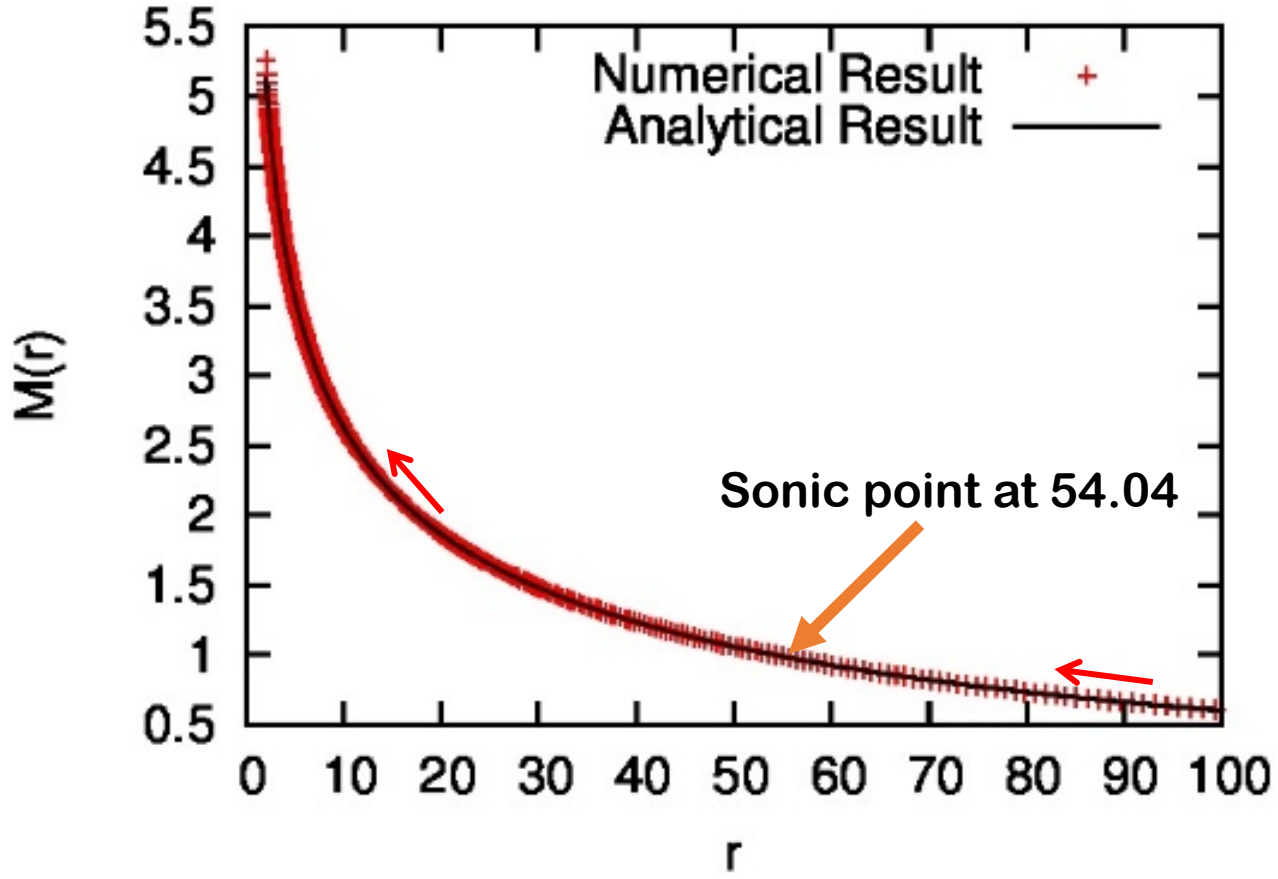

r_{out} = 100 GM/c^2
r_{in} = 2.1 GM/c^2

300 logarithmic zones

Parameters for above simulation: $\varepsilon = 1.015 \Rightarrow V = 0.053$ and $a_s = 0.088$ at $r_{out} = 100$

Results: One Dimensional Axisymmetric Flow

Schwarzschild Space-time

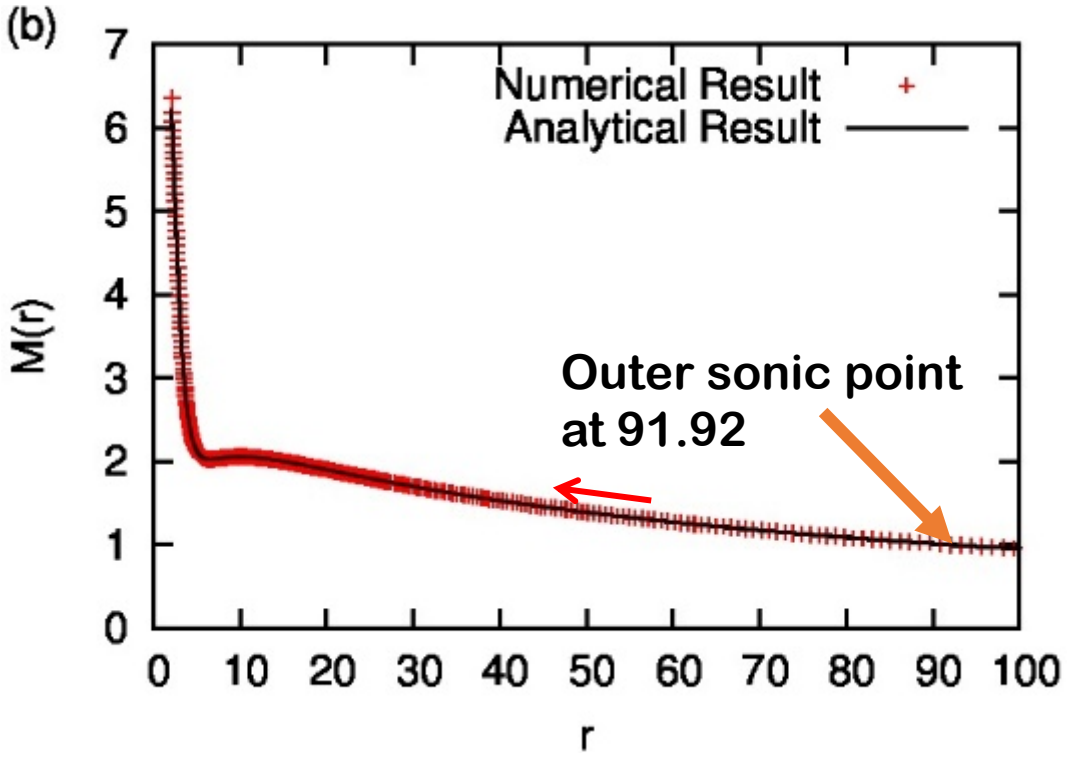

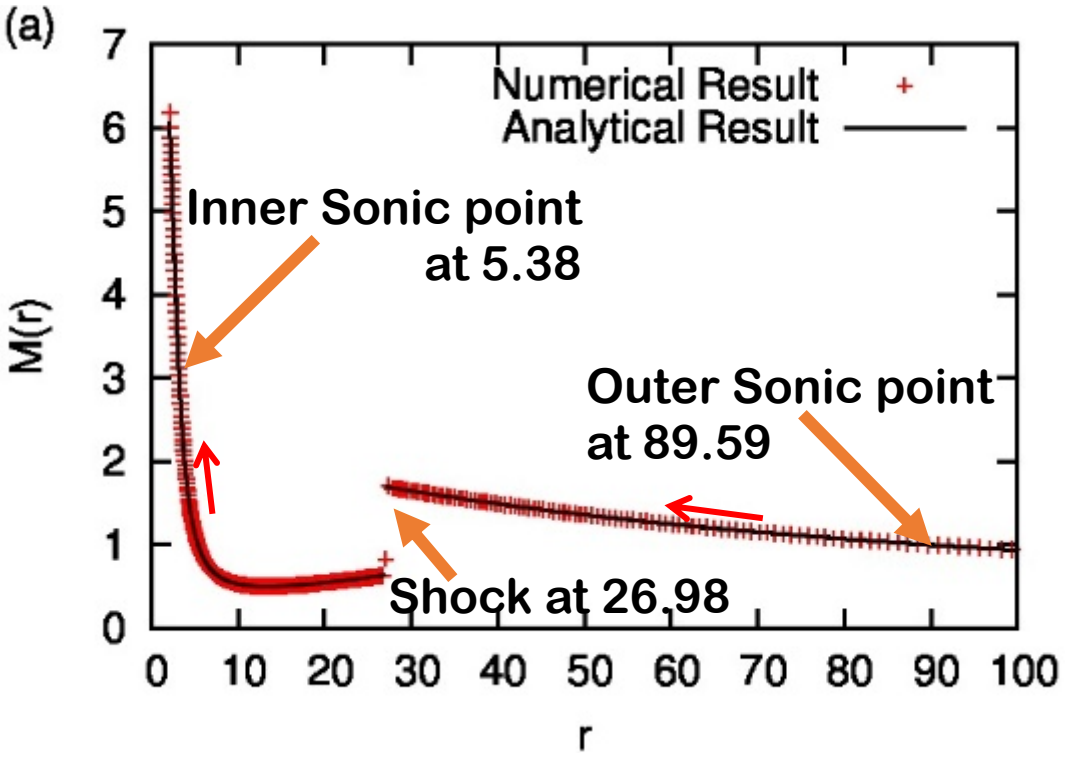

NSA region:
$\varepsilon = 1.007$, $l = 3.25$

SA region:
$\varepsilon = 1.007$, $l = 3.4$

$r_{out} = 100\ GM/c^2$
$r_{in} = 2.1\ GM/c^2$

300 logarithmic zones

Results: One Dimensional Axisymmetric Flow

Kerr Space-time

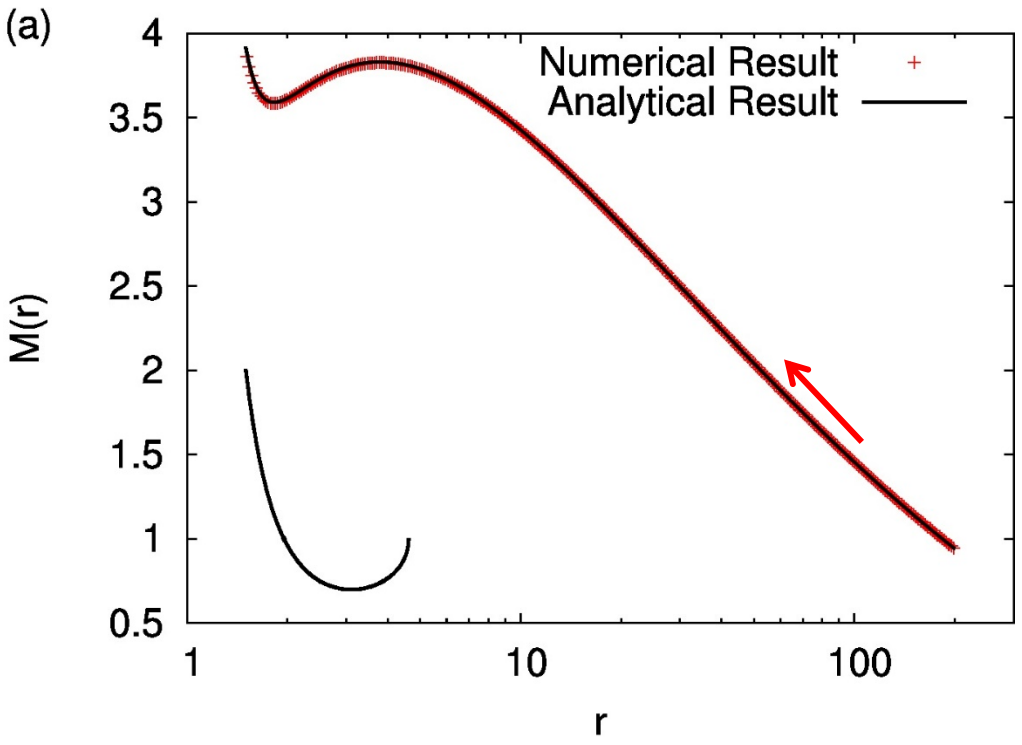

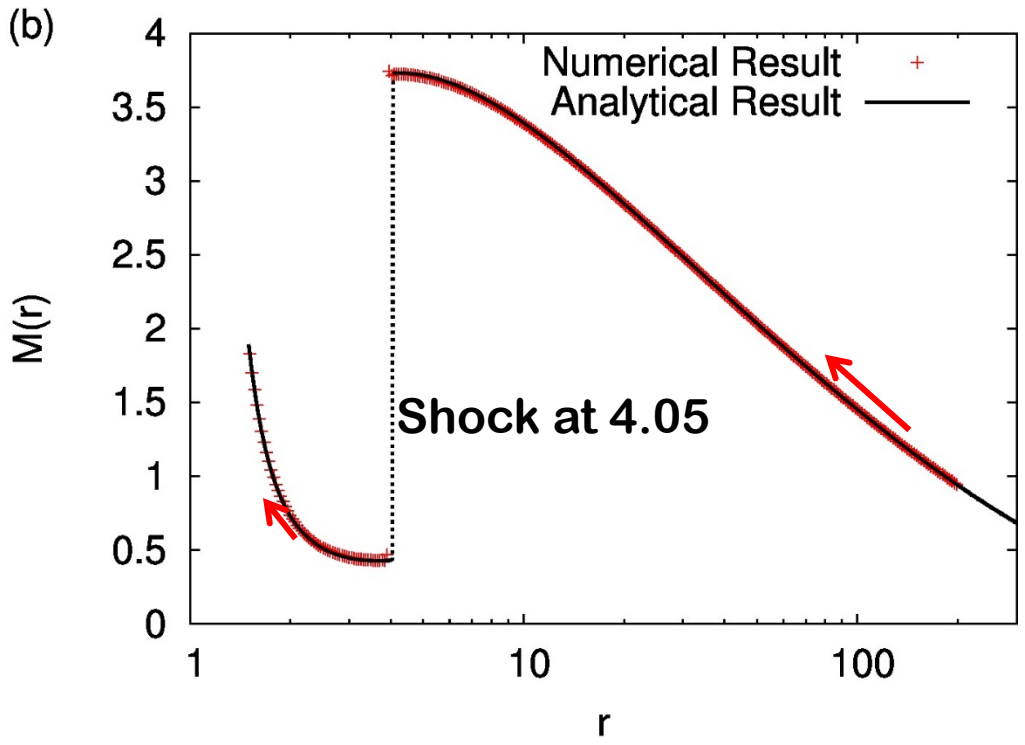

NSA region:
$\varepsilon = 1.004$, $l = 2.2$, $a = 0.95$

SA region:
$\varepsilon = 1.004$, $l = 2.25$, $a = 0.95$

$r_{out} = 200\ GM/c^2$
$r_{in} = 1.5\ GM/c^2$

300 logarithmic zones

Results: One Dimensional Axisymmetric Flow

Kerr Space-time

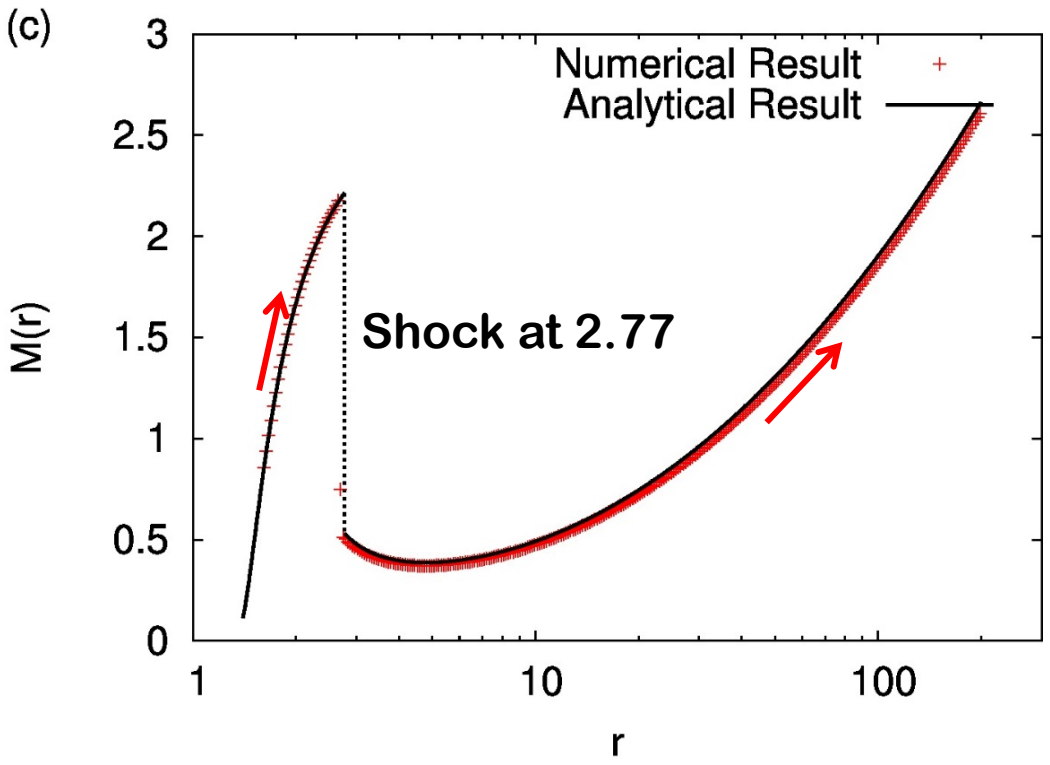

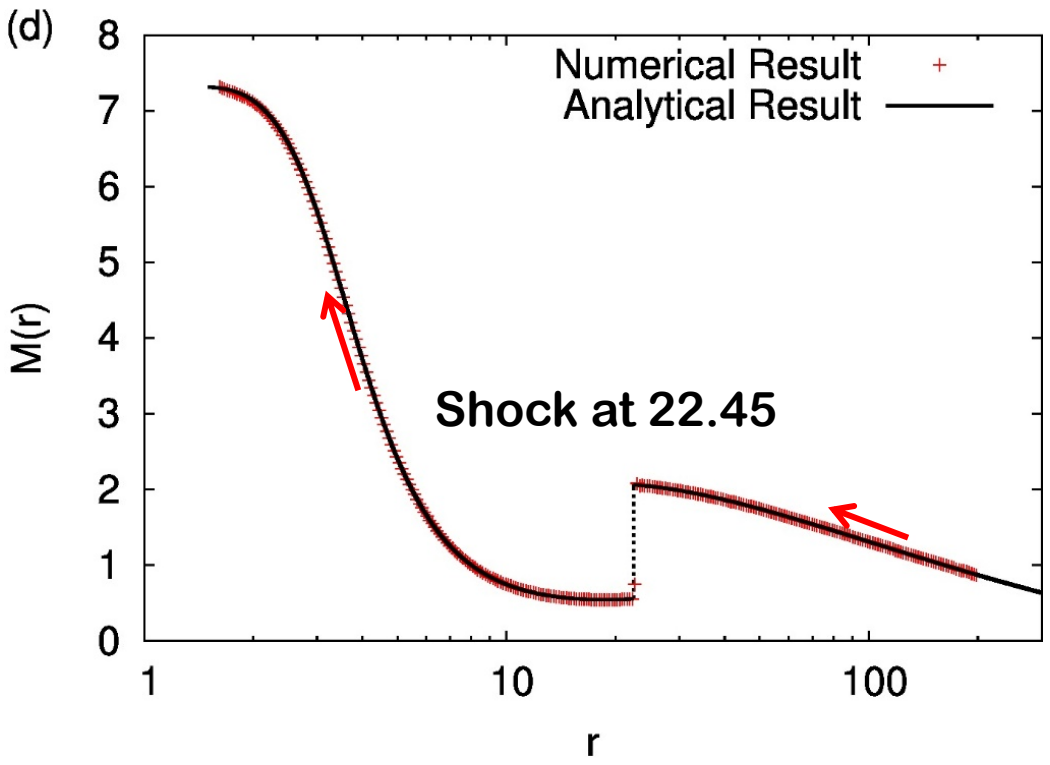

SW region:
$\varepsilon = 1.02$, $l = 2.3$, $a = 0.95$

$r_{in} = 1.5\ GM/c^2$; $r_{out} = 200\ GM/c^2$;
300 logarithmic zones

SA region:
$\varepsilon = 1.004$, $l = 4.0$, $a = -0.95$

$r_{out} = 200\ GM/c^2$; $r_{in} = 1.6\ GM/c^2$;
300 logarithmic zones

Extending beyond 1D

Numerical Simulations

- Numerical simulation of accretion flow which exhibited shocks started since 1970s (Wilson et al. 1972, Hawley et al. 1984).
- Theoretical work made it systematic by properly dividing the parameter space spanned by the specific energy and angular momentum (Fukue 1987, Chakrabarti 1989, 1990)

D. Ryu et al., 1995

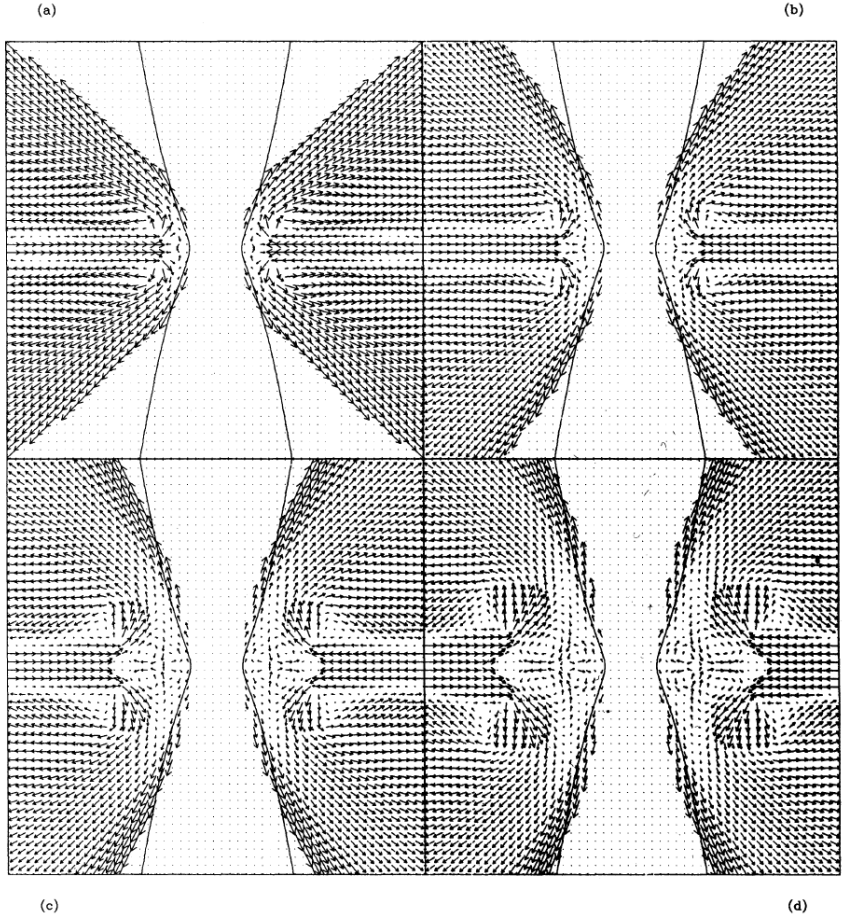

Velocity field at the end of the simulation, in (a) run 1, (b) run 2, (c) run 3, and (d) run 4. The full r-z plane with $4 \leq r \leq 4$, $4 \leq z \leq 4$, is shown. Solid lines show the funnel wall according to eq. (2.13).

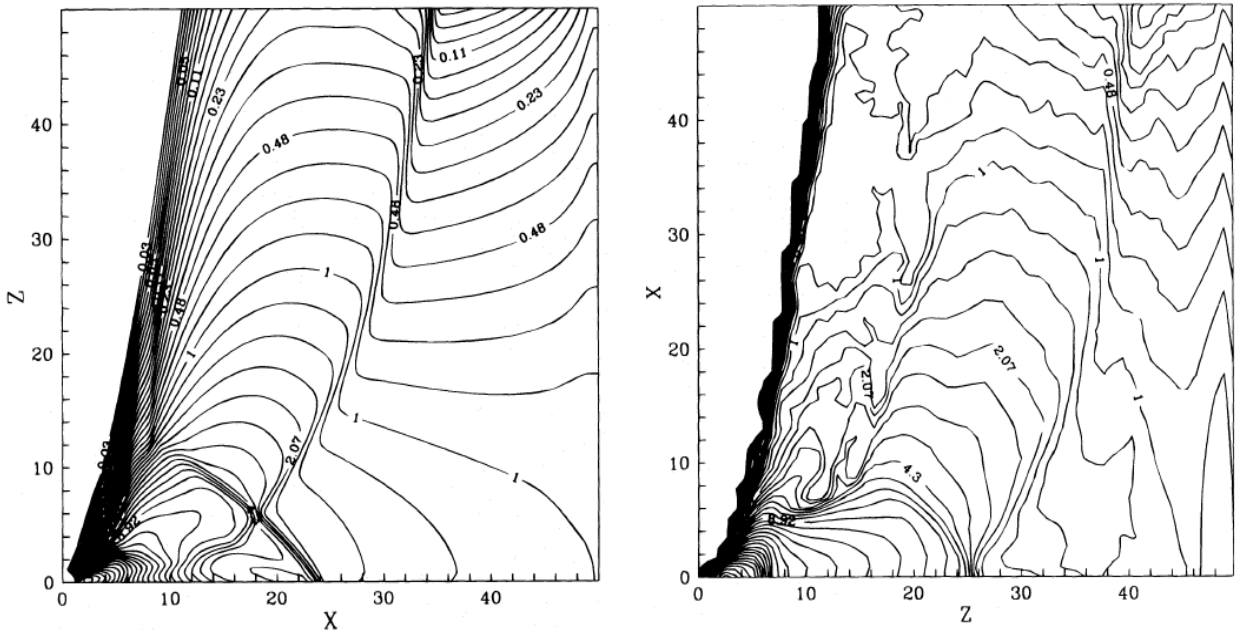

Hydrodynamic simulation of shocked accretion flow using two different simulations codes, one FD-TVD (left) and another SPH (right). Figure is taken from Molteni, Ryu & Chakrabarti, 1996.

TCAF Model to Explain Spectral Properties for Galactic, Extra-galactic and Intermediate Mass Black Holes

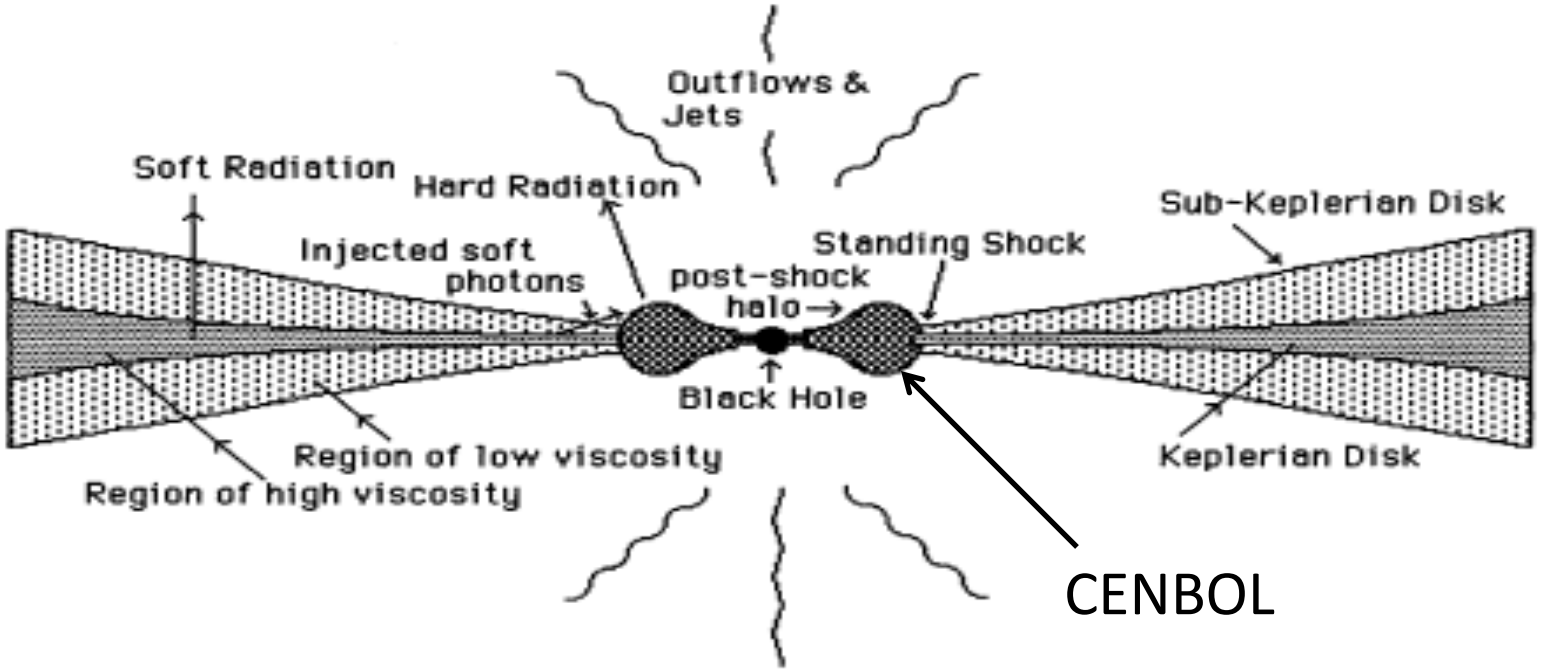

- Two Component Advective Flow (TCAF) – Keplerian and sub-Keplerian
- Centrifugal Pressure Dominated Boundary Layer (CENBOL) forms because of the angular momentum of the sub-Keplerian component
- The CENBOL Comptonizes soft photons from the Keplerian disk and radiates them as the hard photons
- Recently it has been added to XSPEC as an additive table model

Chakrabarti & Titarchuk, ApJ, 1995

Formation of TCAF using numerical simulation

Using suitable viscosity parameters and cooling processes, it is possible to simulate stable TCAF configuration (Giri & Chakrabarti, 2013; Giri, Garain & Chakrabarti, 2015).

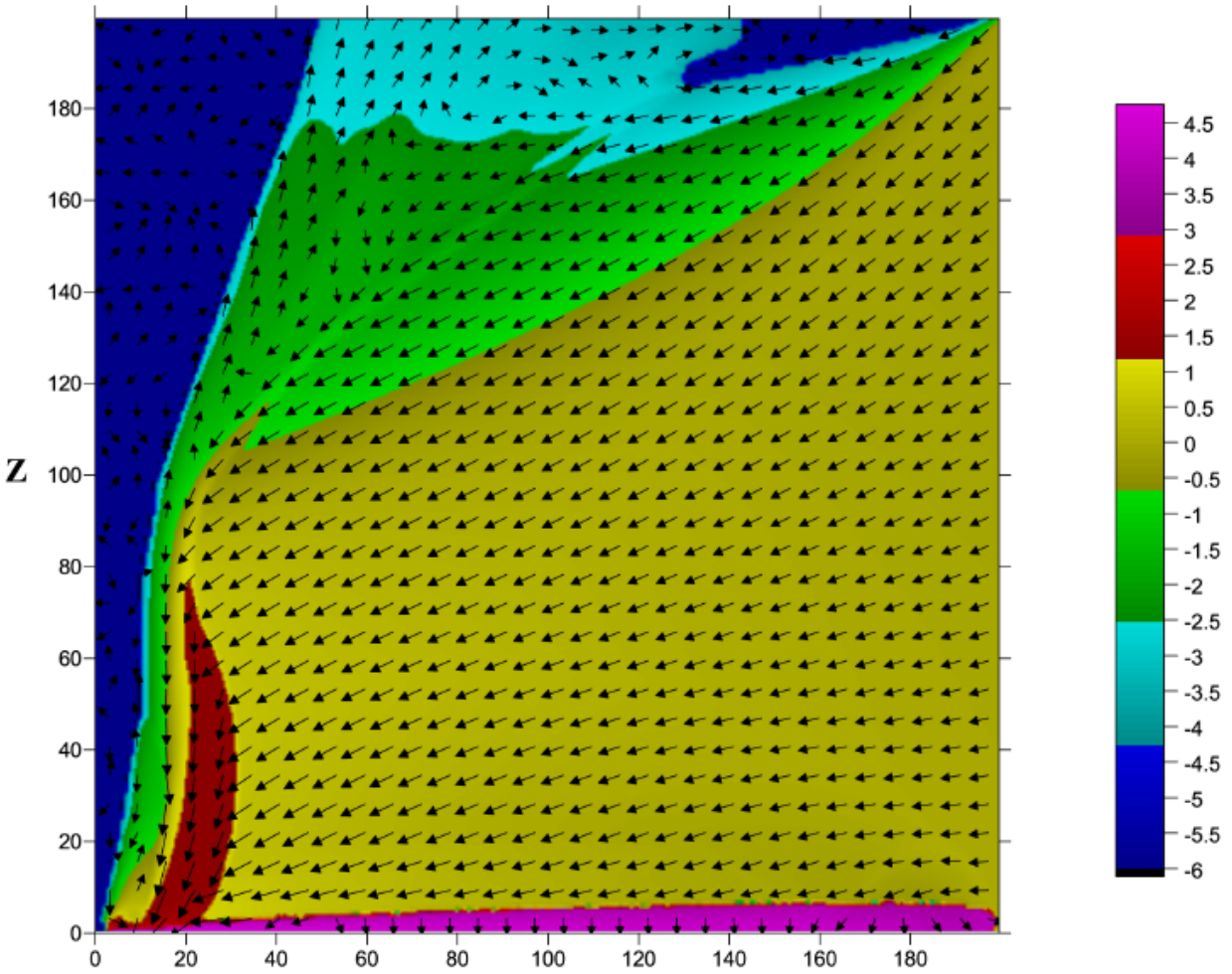

Density overlaid with velocity vectors

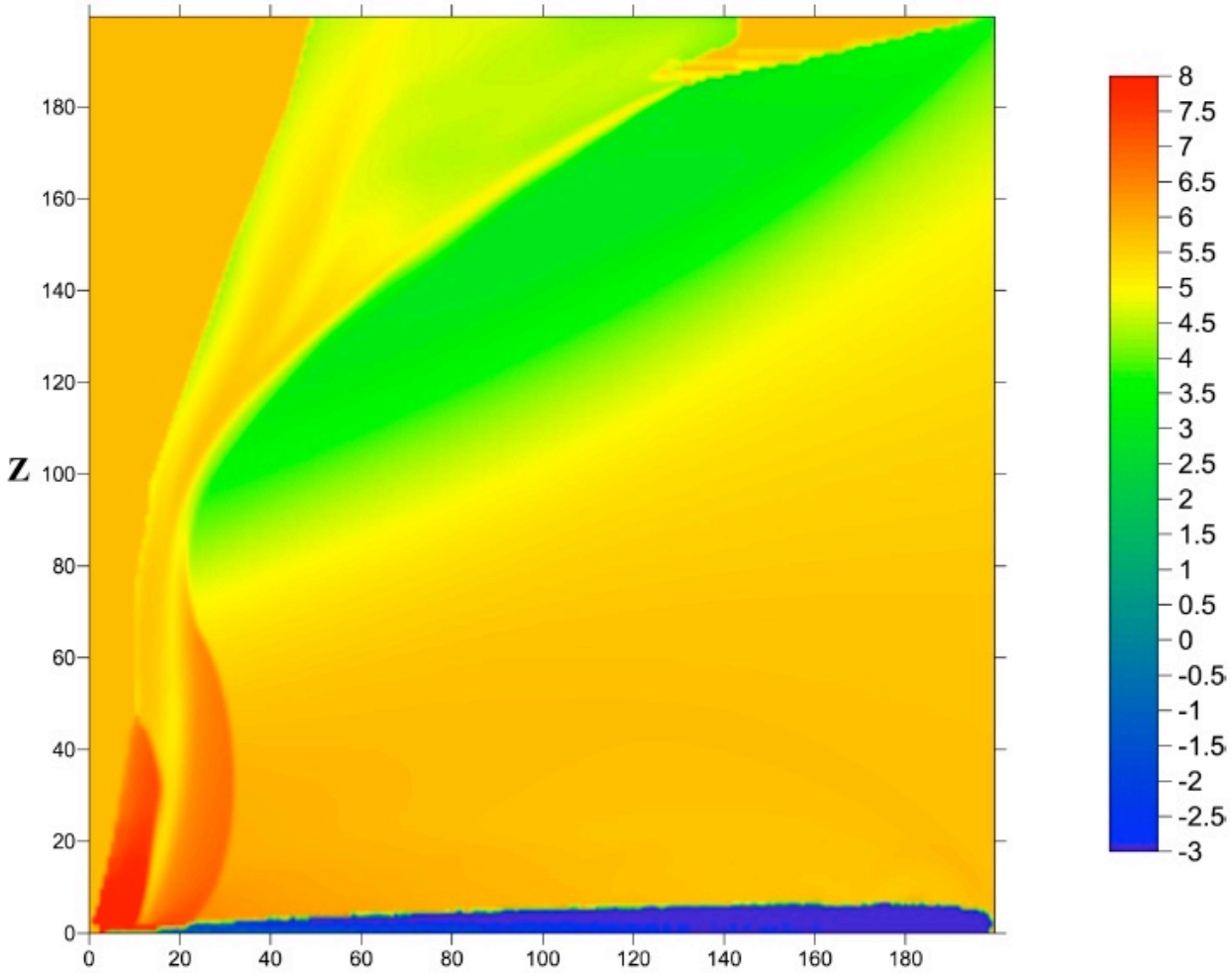

Temperature distribution

MNRAS 466, 1372–1381 (2017) doi:10.1093/mnras/stw3117
Advance Access publication 2016 December 1

The 2004 outburst of BHC H1743-322: analysis of spectral and timing properties using the TCAF solution

Ayan Bhattacharjee,[1]★ Indrani Banerjee,[1] Anuvab Banerjee,[1] Dipak Debnath[2]★ and Sandip K. Chakrabarti[1,2]★

MNRAS 460, 3163–3169 (2016) doi:10.1093/mnras/stw860
Advance Access publication 2016 April 15

Estimation of the mass of the black hole candidate MAXI J1659−152 using TCAF and POS models

Aslam Ali Molla,[1] Dipak Debnath,[1]★ Sandip K. Chakrabarti,[1,2] S. Mondal[1] and A. Jana[1]

MNRAS 447, 1984–1995 (2015) doi:10.1093/mnras/s

Characterization of GX 339-4 outburst of 2010–11: analysis by XSPEC using two component advective flow model

Dipak Debnath,[1]★ Santanu Mondal[1] and Sandip K. Chakrabarti[1,2]

The Astrophysical Journal, 834:88 (12pp), 2017 January 1 doi:10.3847/1538-4357/834/1/88

ESTIMATION OF MASS OF COMPACT OBJECT IN H 1743-322 FROM 2010 AND 2011 OUTBURSTS USING TCAF SOLUTION AND SPECTRAL INDEX–QPO FREQUENCY CORRELATION

Aslam Ali Molla[1], Sandip K. Chakrabarti[1,2], Dipak Debnath[1], and Santanu Mondal[1,3]

The Astrophysical Journal, 850:91 (7pp), 2017 November 20 https://doi.org/10.3847/1538-4357/aa88a5

Properties of X-Ray Flux of Jets during the 2005 Outburst of Swift J1753.5−0127 Using the TCAF Solution

Arghajit Jana[1], Sandip K. Chakrabarti[1,2], and Dipak Debnath[1]

The Astrophysical Journal, 850:92 (11pp), 2017 November 20 https://doi.org/10.3847/1538-4357/aa9077

Accretion Flow Properties of Swift J1753.5-0127 during Its 2005 Outburst

Dipak Debnath[1], Arghajit Jana[1], Sandip K. Chakrabarti[1,2], Debjit Chatterjee[1], and Santanu Mondal[1,3]

The Astrophysical Journal, 827:88 (7pp), 2016 August 10

ACCRETION FLOW PROPERTIES OF MAXI J1543–564 DURING 2011 OUTBURST FROM THE TCAF SOLUTION

Debjit Chatterjee[1], Dipak Debnath[1,2], Sandip K. Chakrabarti[1,3], Santanu Mondal[1,4], and Arghajit Jana[1]

Accretion onto non-rotating black hole in 2D

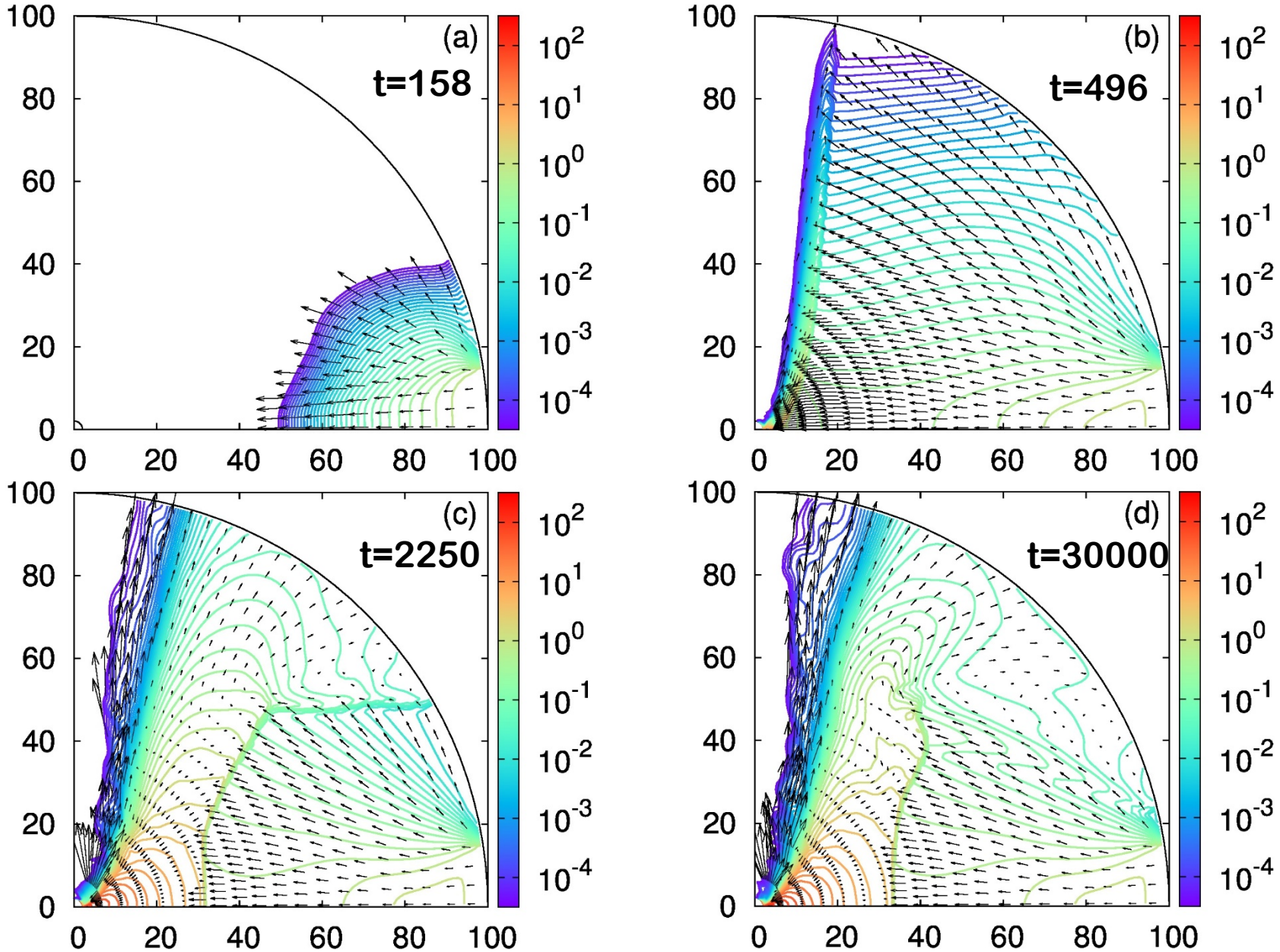

r_{out} = 100 GM/c^2
r_{in} = 2.1 GM/c^2

300 logarithmic radial zones

100 equi-spaced zones in polar direction

Axi-symmetric Prograde Accretion

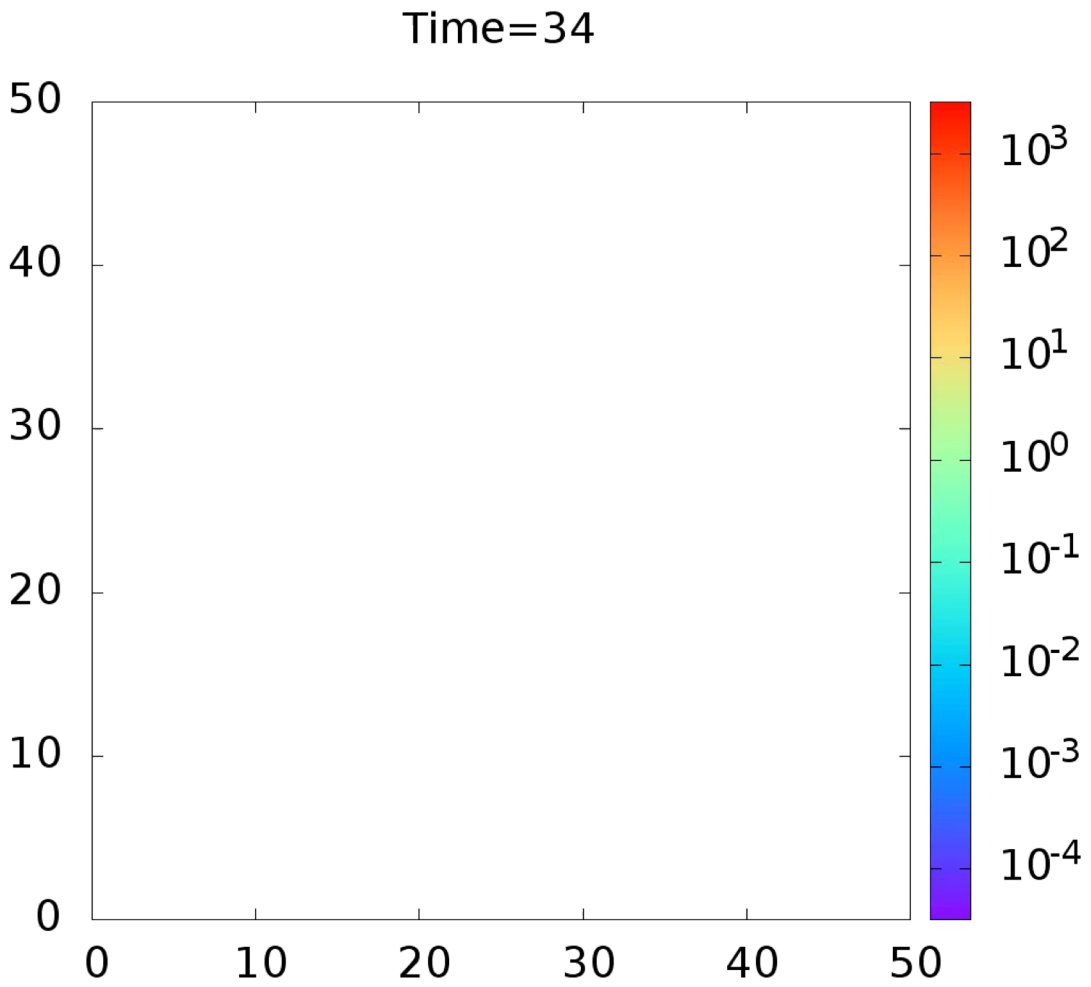

r_{out} = 200 GM/c^2
r_{in} = 1.5 GM/c^2

300 logarithmic radial zones

90 equi-spaced zones in polar direction

Parameters chosen from SA region of vertical equilibrium model: ε = 1.001, l = 2.25, a = 0.95

Axi-symmetric Prograde Accretion

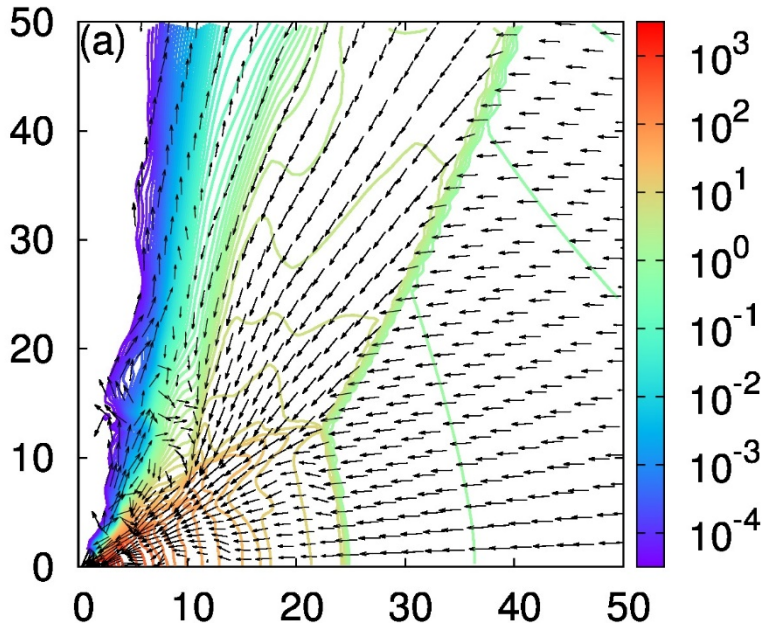

Density contours over-plotted with velocity vectors at final time

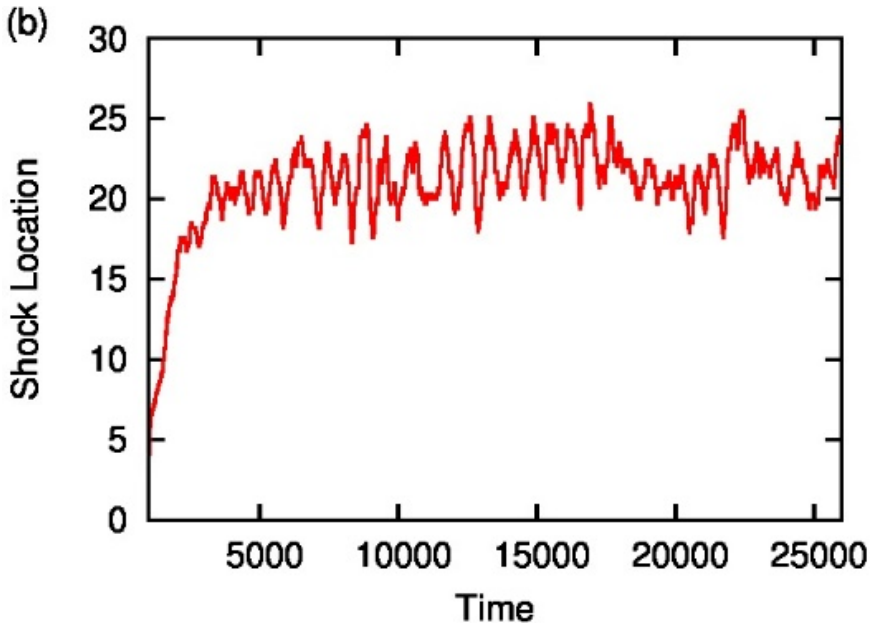

Time variation of the shock location on the equatorial plane

Parameters chosen from SA region of vertical equilibrium model: $\varepsilon = 1.001$, $l = 2.25$, $a = 0.95$

Axi-symmetric Prograde Accretion

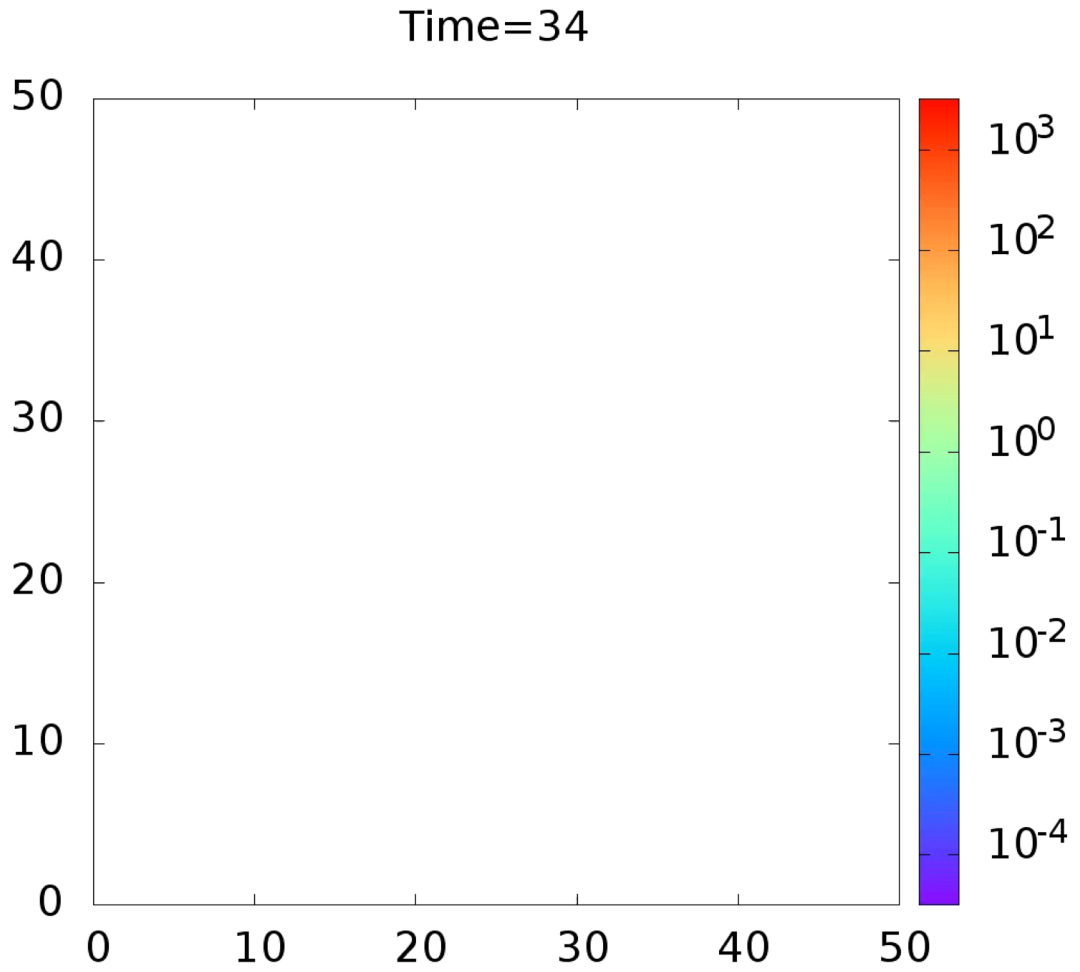

r_{out} = 200 GM/c^2
r_{in} = 1.5 GM/c^2

300 logarithmic radial zones

90 equi-spaced zones in polar direction

Parameters chosen from NSA region of vertical equilibrium model: ε = 1.001, l = 2.21, a = 0.95

Axi-symmetric Prograde Accretion

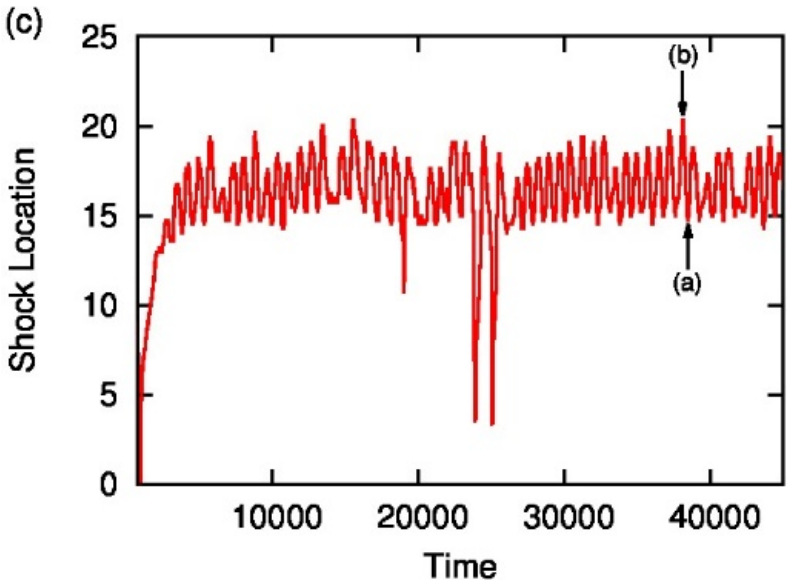

Time variation of the shock location on the equatorial plane

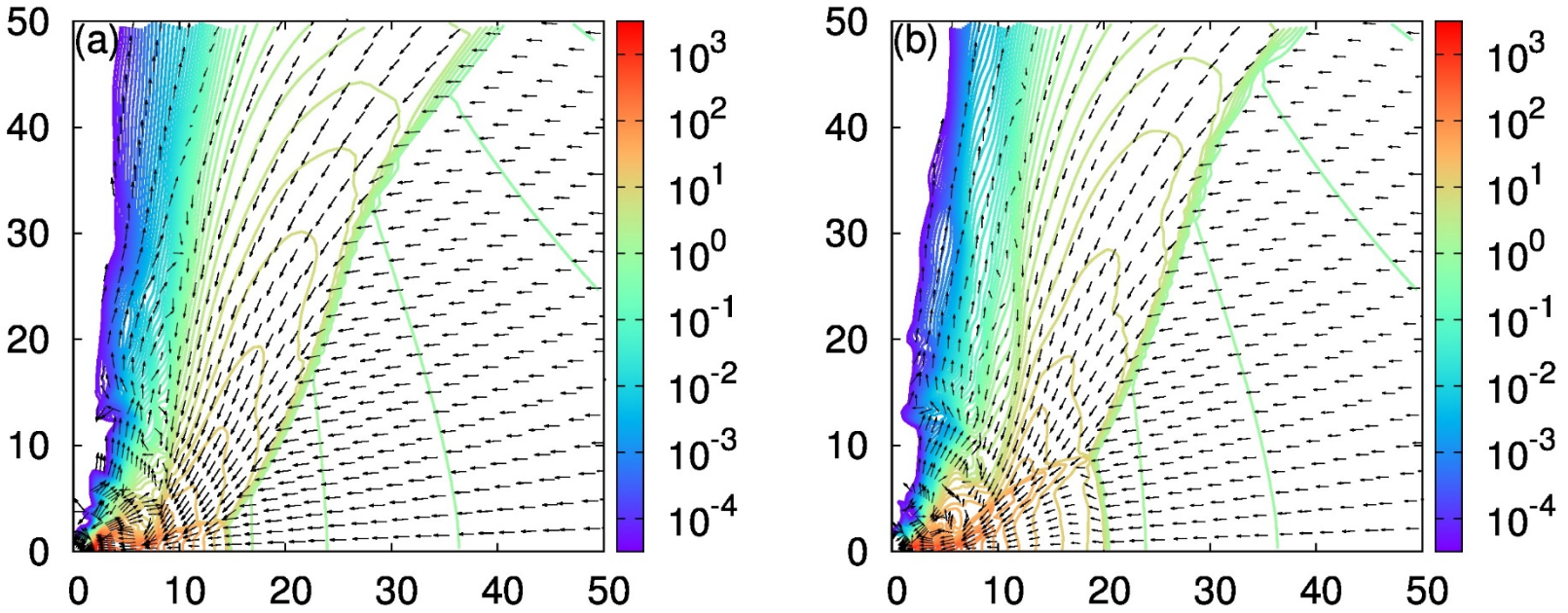

Density contours over-plotted with velocity vectors at two times marked by arrows

Parameters chosen from NSA region of vertical equilibrium model: $\varepsilon = 1.001$, $l = 2.21$, $a = 0.95$

Axi-symmetric Retrograde Accretion

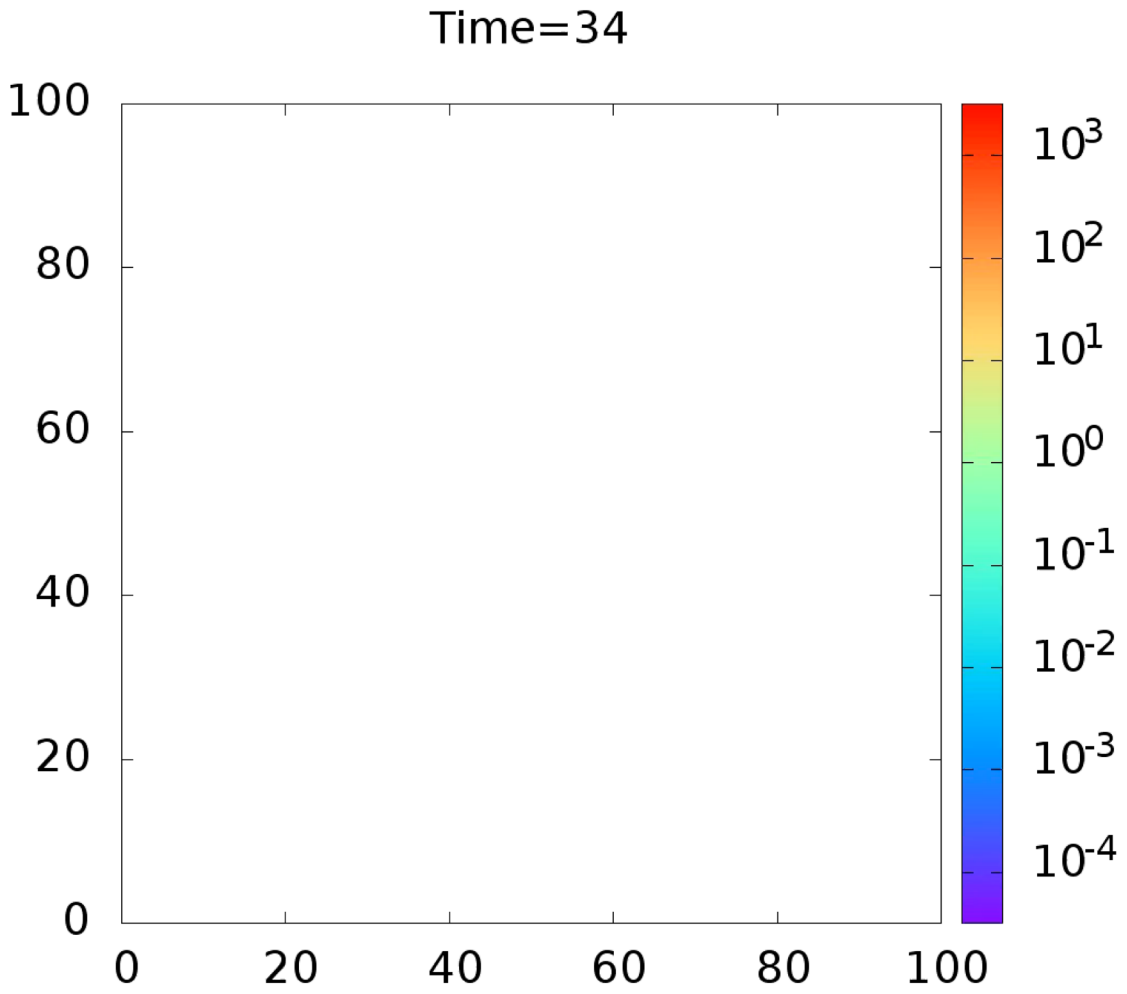

r_{out} = 200 GM/c^2
r_{in} = 1.5 GM/c^2

300 logarithmic radial zones

90 equi-spaced zones in polar direction

Parameters chosen from SA region of vertical equilibrium model: ε = 1.001, l = 4.0, a = -0.95

Axi-symmetric Retrograde Accretion

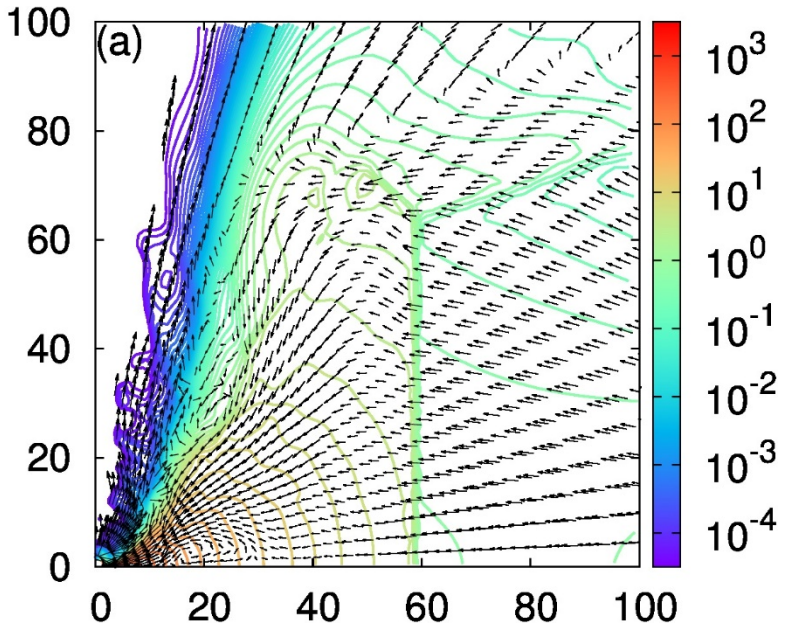

Density contours over-plotted with velocity vectors at final time

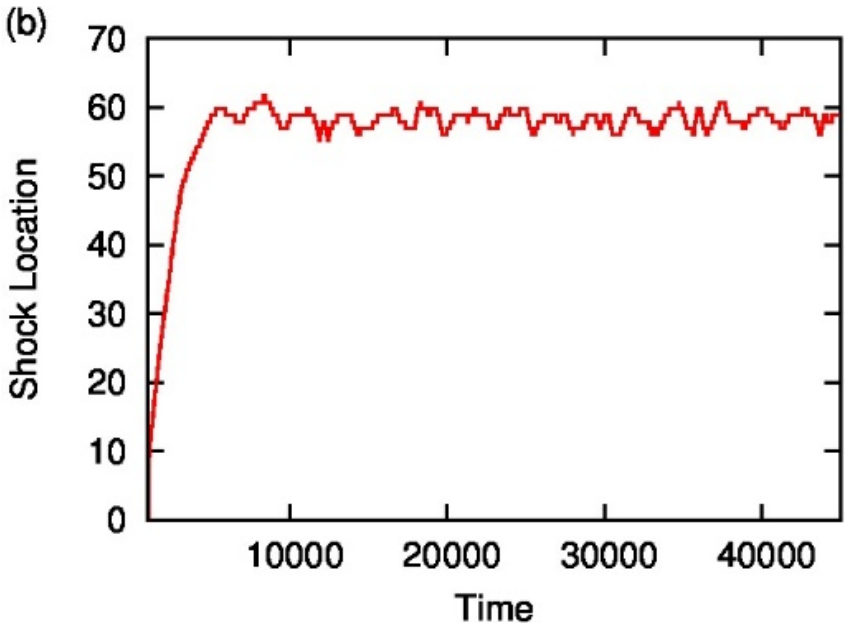

Time variation of the shock location on the equatorial plane

Parameters chosen from SA region of vertical equilibrium model: ε = 1.001, l = 4.0, a = -0.95

Axi-symmetric Prograde Accretion

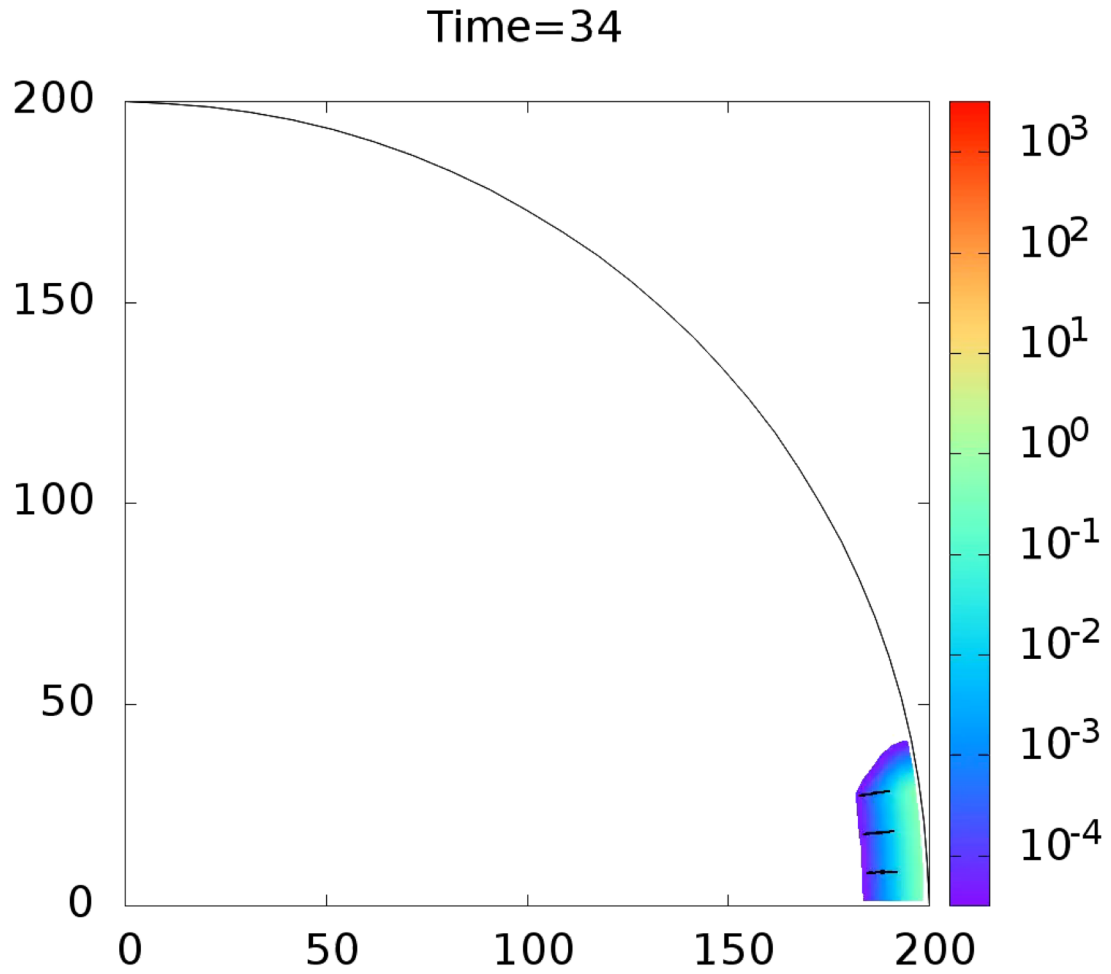

r_{out} = 200 GM/c^2
r_{in} = 1.5 GM/c^2

300 logarithmic radial zones

90 equi-spaced zones in polar direction

Parameters chosen from O* region of vertical equilibrium model: ε = 1.001, l = 2.63, a = 0.95

Axi-symmetric Prograde Accretion

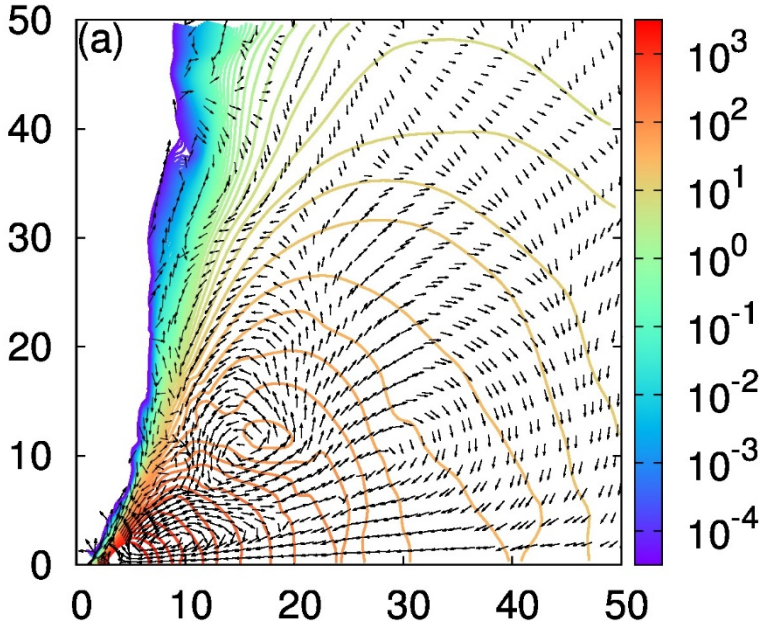

Density contours over-plotted with velocity vectors at final time

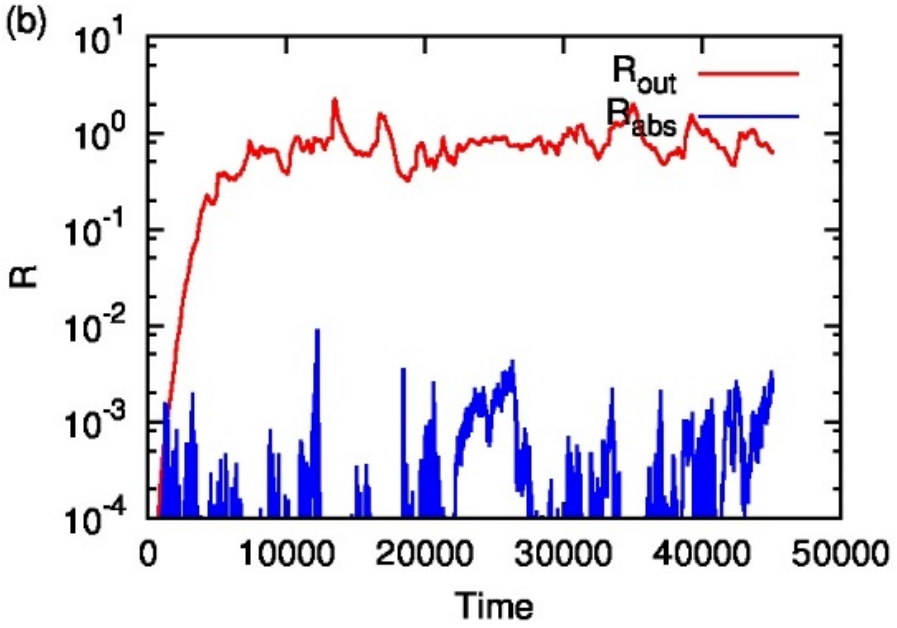

Time variation of the ratio $R_{out}=\dot{M}_{outflow}/\dot{M}_{inflow}$ and $R_{abs}=\dot{M}_{absorption}/\dot{M}_{inflow}$

Parameters chosen from O* region of vertical equilibrium model: $\varepsilon = 1.001$, $l = 2.63$, $a = 0.95$

MHD Simulation for Axi-symmetric Accretion on to a Black Hole (non-GR)

Lower specific angular momentum $\lambda = 1.5$

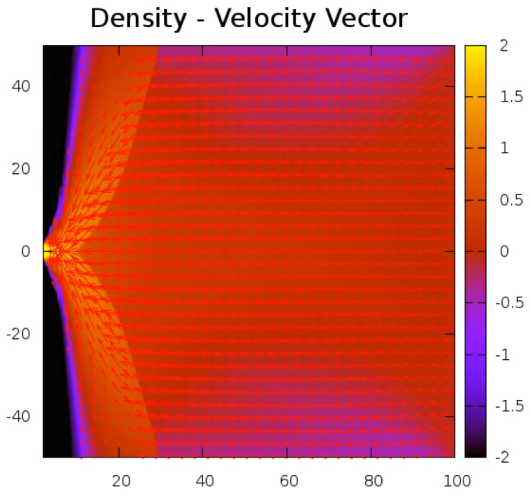

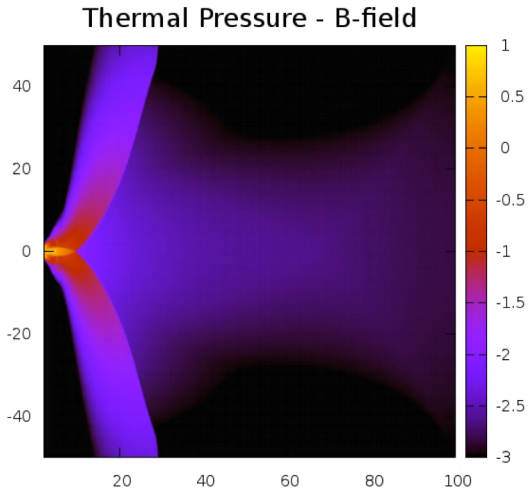

Higher specific angular momentum $\lambda = 1.65$

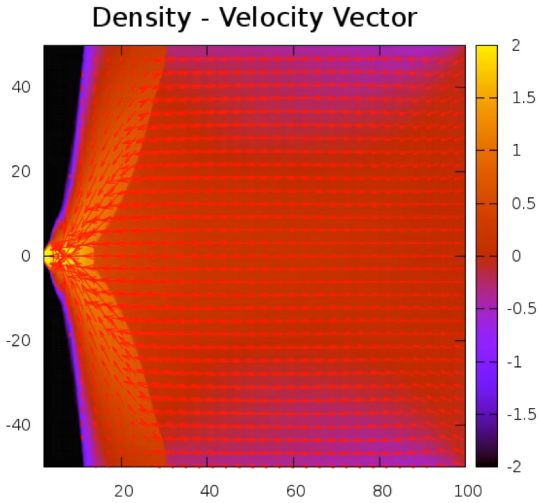

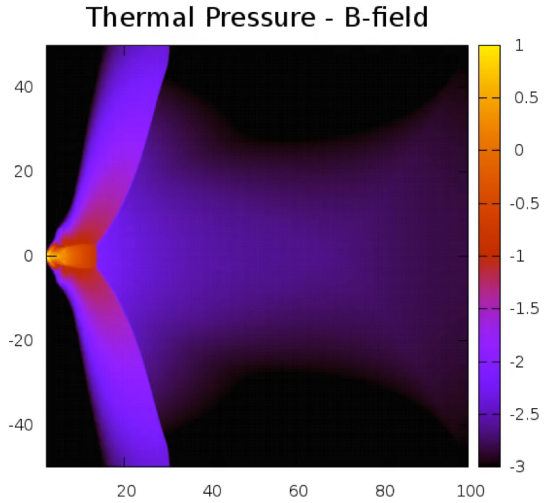

Garain, Balsara, Chakrabarti, Kim, 2019

Fluid dynamics code can be coupled with (Monte Carlo based) radiative transfer code to simulate dynamics as well as spectral and timing properties of accretion disk (non-GR).

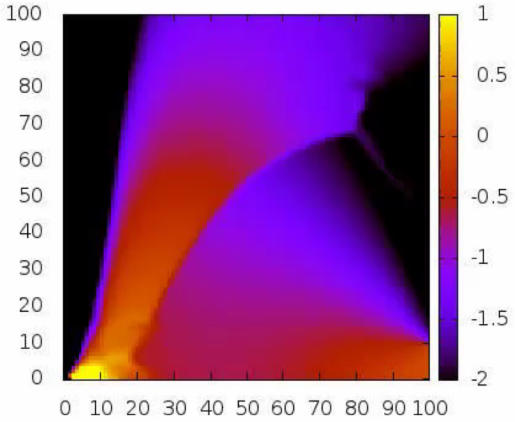

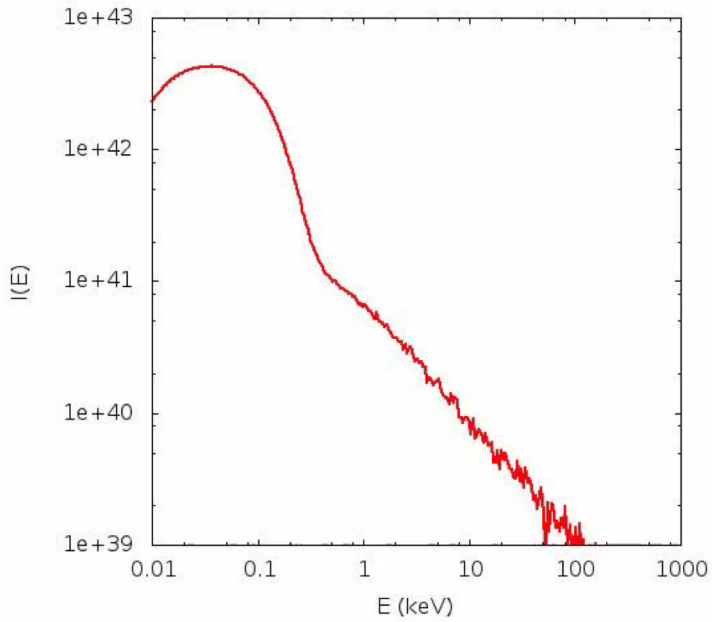

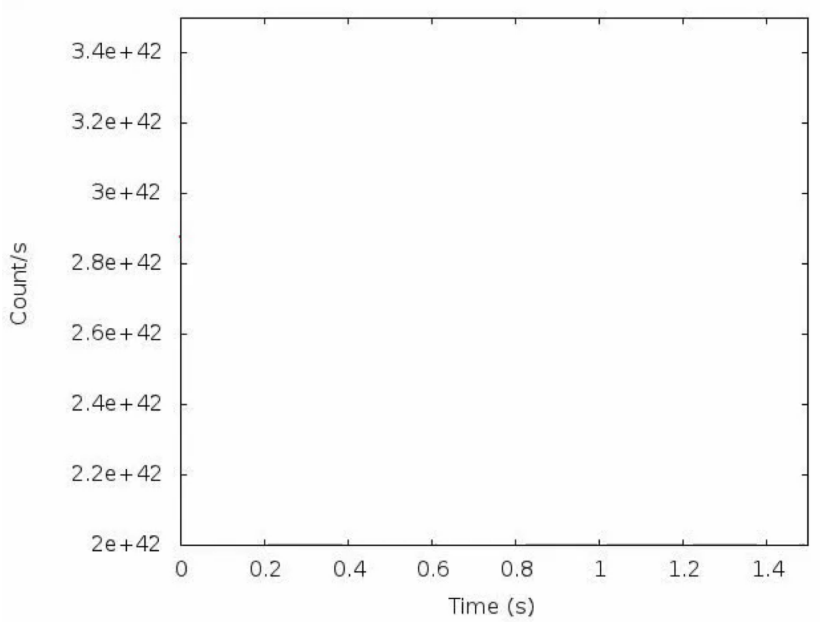

Garain, Ghosh, Chakrabarti, 2014, MNRAS

Timing Properties: Light Curves and Power Density Spectra

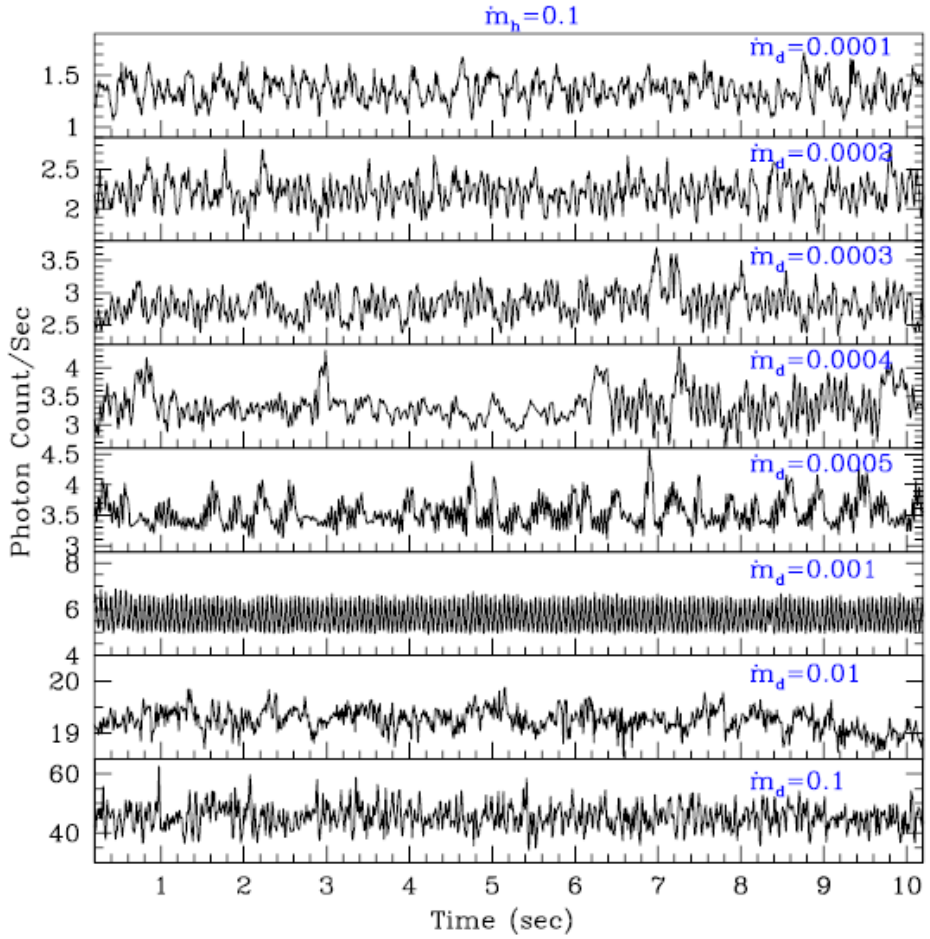

Time variation of photon count rate (in unit of 10^{42})

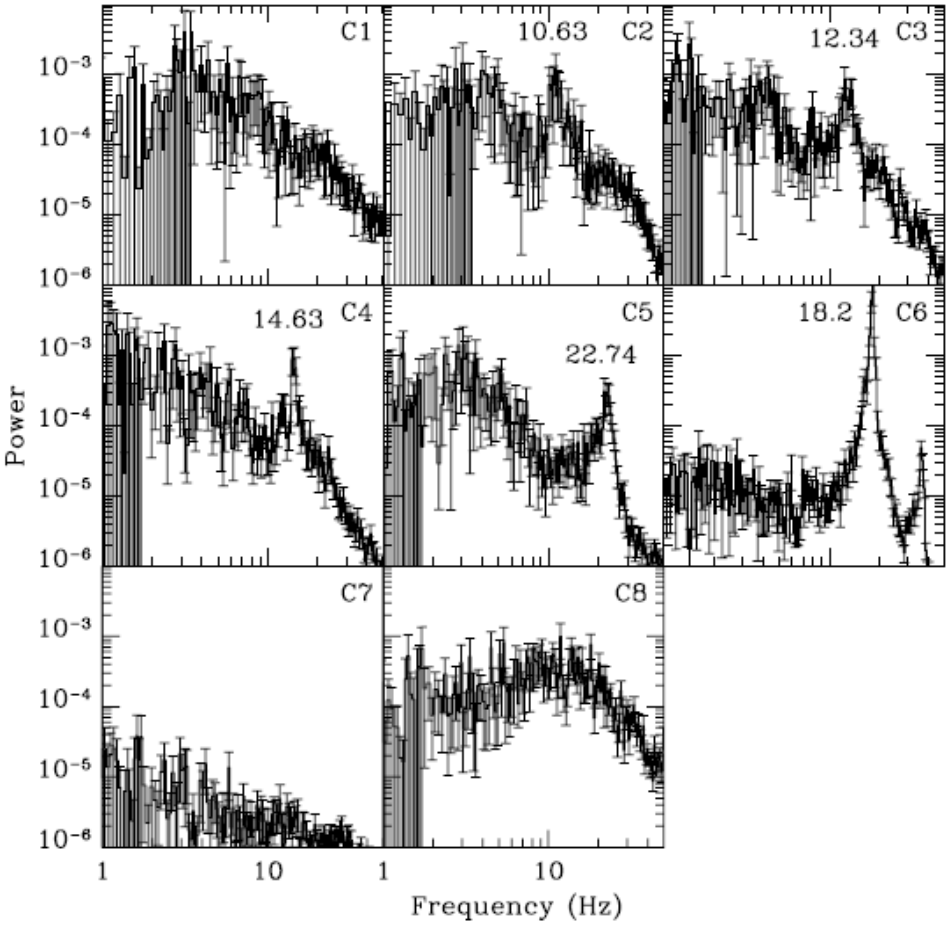

PDS show LFQPOs

Garain, Ghosh, Chakrabarti, MNRAS, 2014

3D Spherically Symmetric Bondi Accretion onto non-rotating Black Hole (non-GR)

Simulation performed on a spherical geodesic mesh with angular resolution of 4.3^o and 64 logarithmically binned radial zones: $r_{min} = 2.0$ and $r_{max} = 50.0$

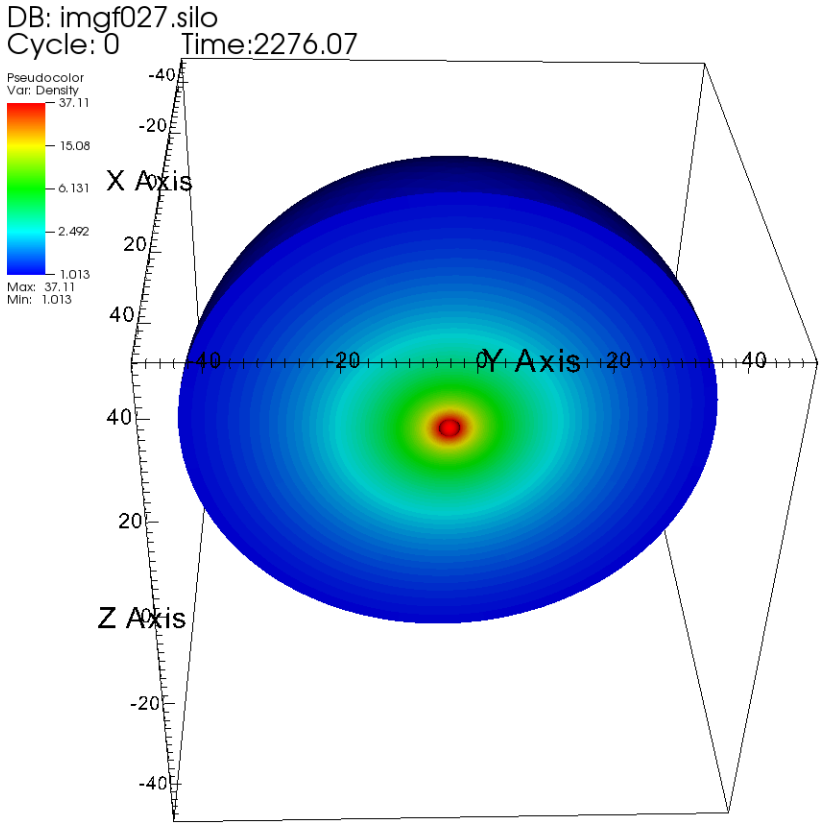

Density clip

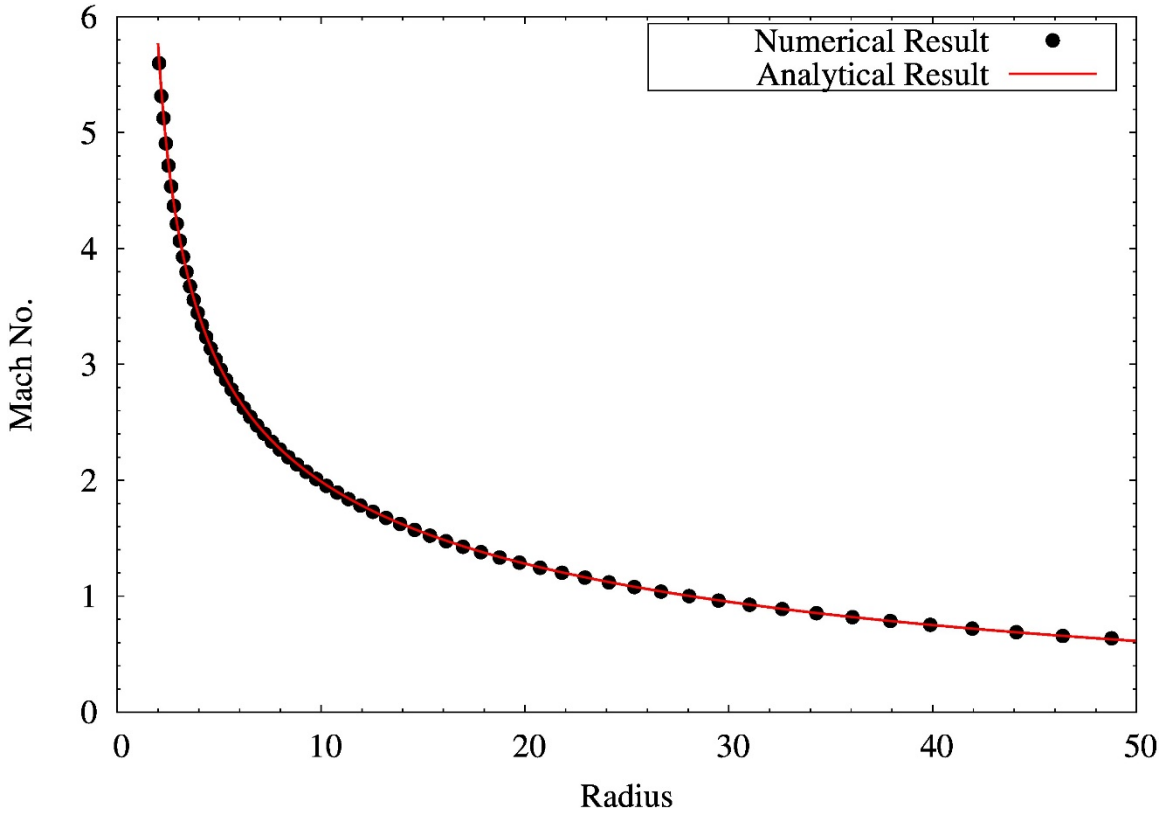

Radial variation of Mach number

Sub-Kepleran Accretion onto non-rotating black hole: 3D Simulation (non-GR)

Specific angular momentum $\lambda = 1.5$

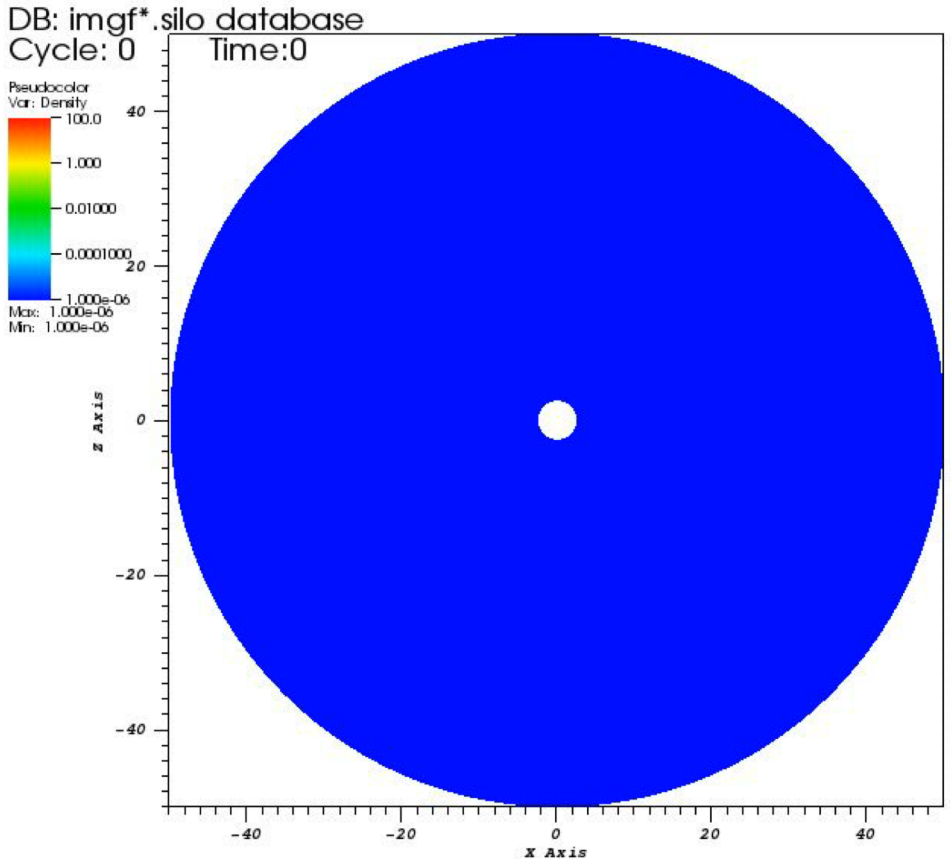

Meridional slice

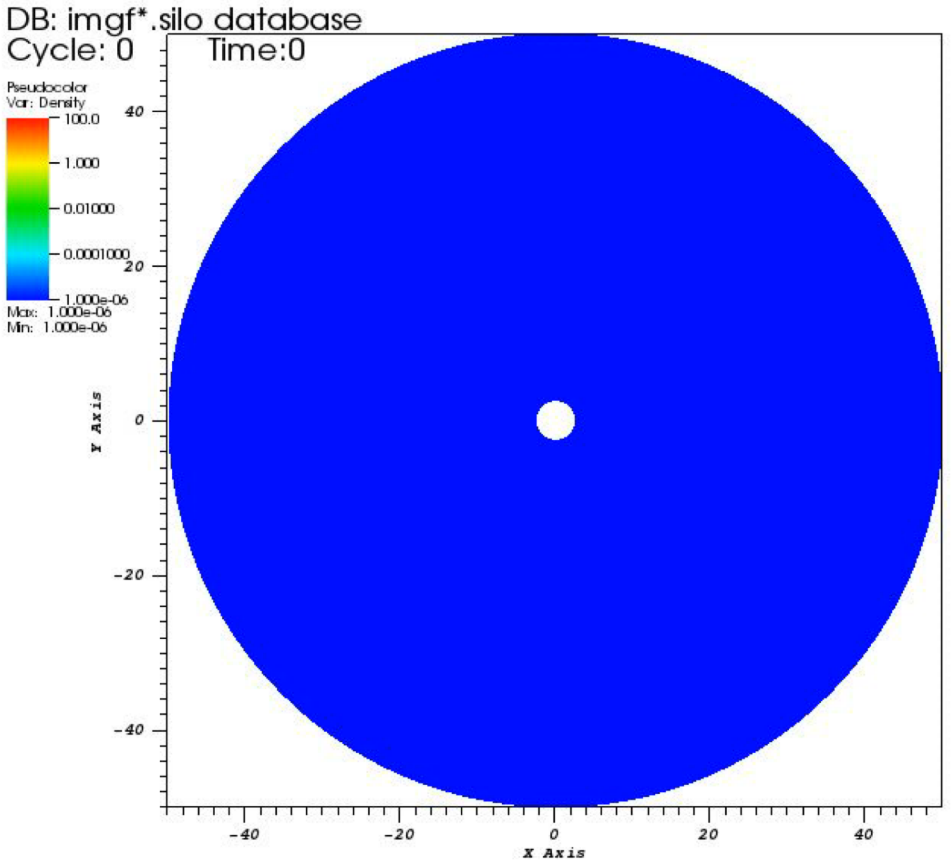

Equatorial slice

Simulation performed on a spherical geodesic mesh with angular resolution of 2.1^o and 200 logarithmically binned radial zones: $r_{min} = 2.0$ and $r_{max} = 50.0$

Simulated images of steady TCAF configuration

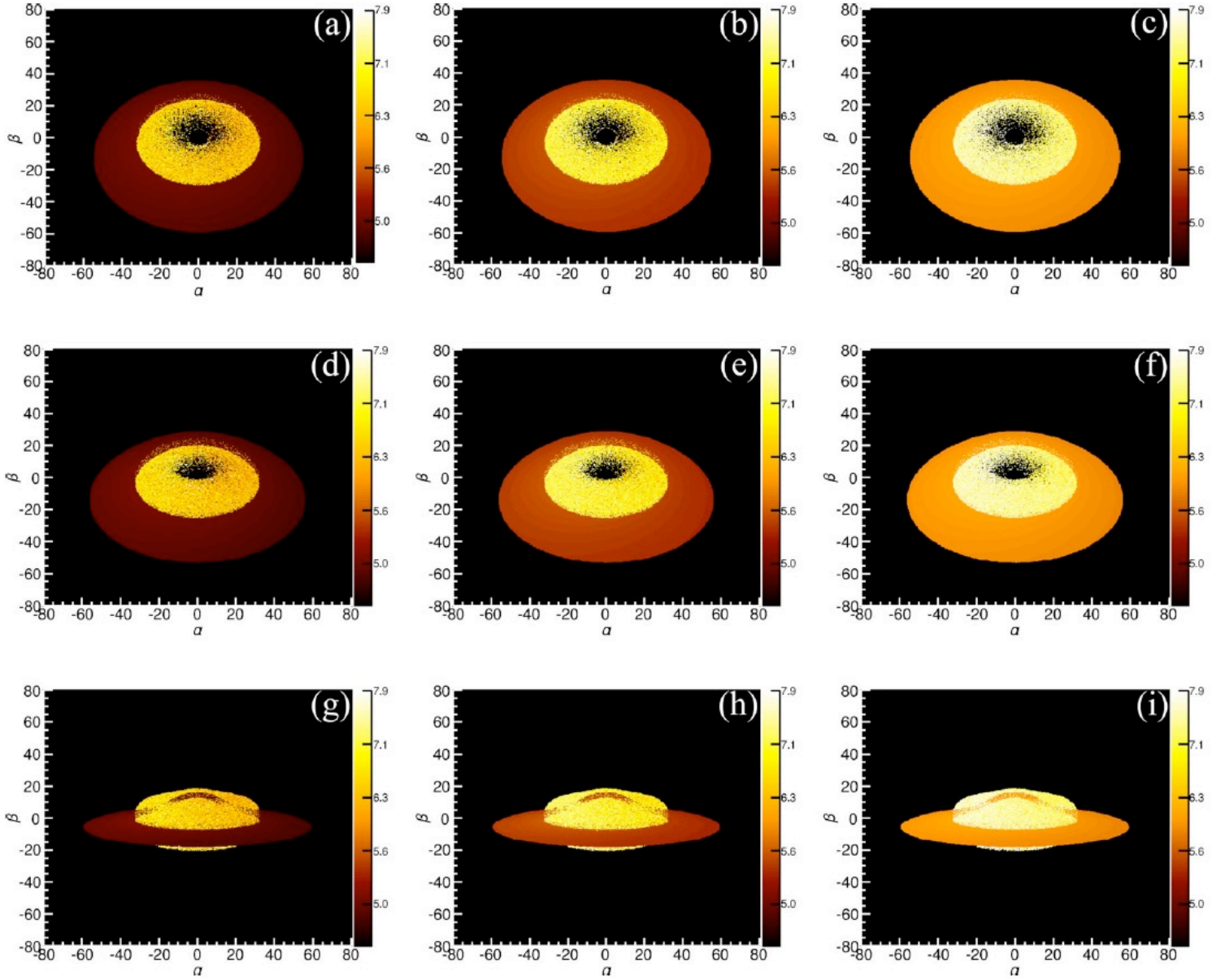

Chatterjee, Ghosh, Chakrabarti, 2017, MNRAS

Figure 9. Images seen by observers from (top panel) 36°, 50° (middle panel) and 80° (bottom panel). Disc rates in the first, second and last columns are $\dot{m}_d = 0.000\,01$, $\dot{m}_d = 0.001$ and $\dot{m}_d = 0.1$, respectively. Colour bar is plotted in the $\log(T_{obs})$ scale with $10^{4.5}$–$10^{7.9}$ K is the range fixed for each panel.

Simulated images of dynamical TCAF configuration

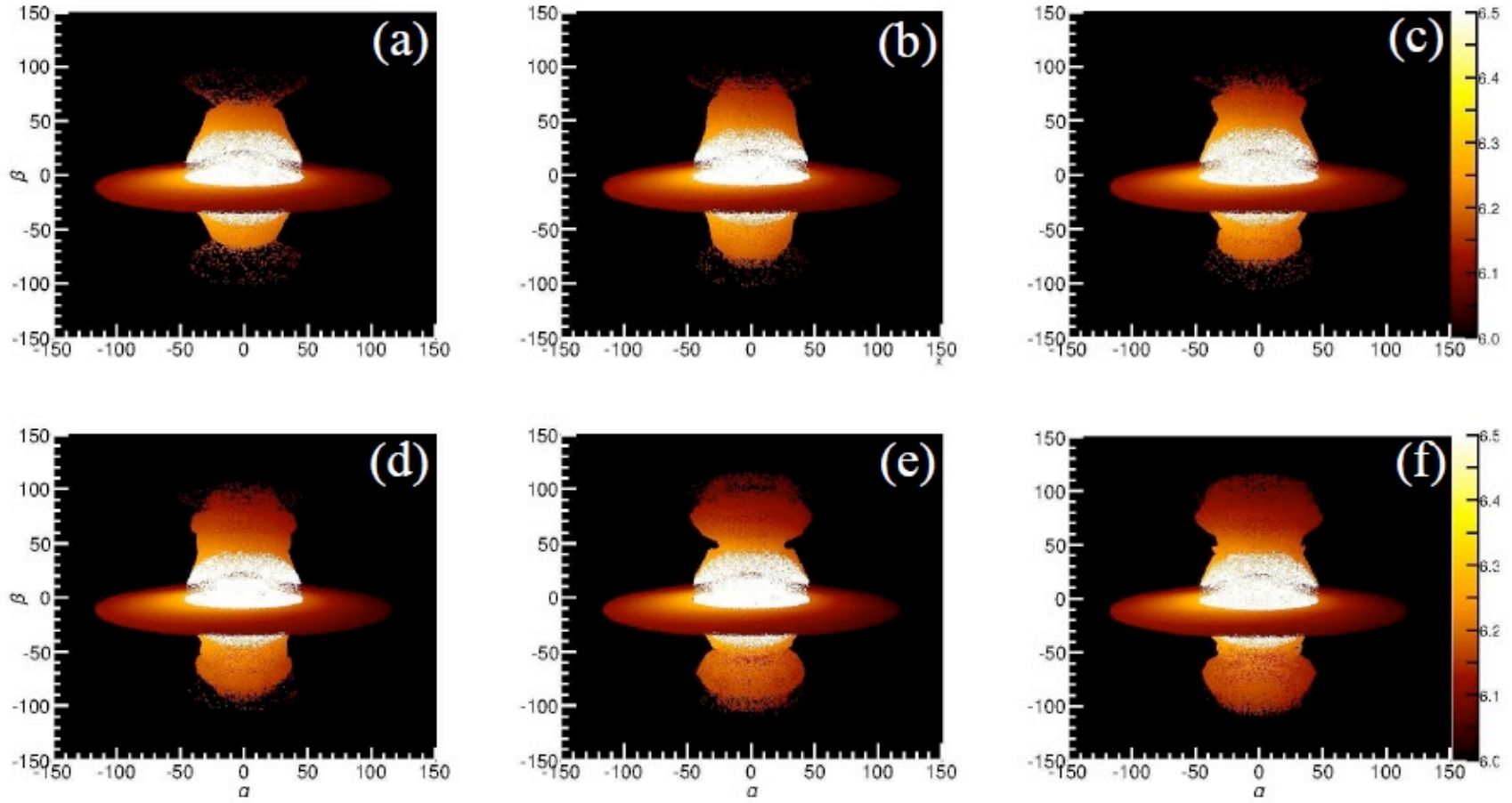

Figure 8. Images of TCAF (in $log(T_{obs})$ scale) in presence of outflows at $t = 14.25s$, $t = 14.35s$, $t = 14.45s$, $t = 14.55s$, $t = 14.65s$ and $t = 14.75s$. Colorbar is in the range $10^{6.0} - 10^{6.5}$ Kelvin and inclination of the observer is at 80°. Asymmetry in the shape is due to difference in Doppler shifts in upper and lower jet components.

Chatterjee+, 2018, MNRAS

Future Research Interest on accretion disk

- 3D GR(M)HD simulations for studying disk dynamics around compact objects
- Inclusion of ray tracing algorithm in Monte Carlo simulation and construct dynamic images of accretion disk
- Numerical technique development for polarization study